



This discussion paper is/has been under review for the journal Atmospheric Measurement Techniques (AMT). Please refer to the corresponding final paper in AMT if available.

What is the benefit of ceilometers for aerosol remote sensing? An answer from EARLINET

M. Wiegner¹, F. Madonna², I. Binietoglou², R. Forkel³, J. Gasteiger¹, A. Geiß¹, G. Pappalardo², K. Schäfer³, and W. Thomas⁴

¹Ludwig-Maximilians-Universität (LMU), Meteorologisches Institut, Theresienstraße 37, 80333 München, Germany

²Consiglio Nazionale delle Ricerche, Istituto di Metodologie per l'Analisi Ambientale (CNR-IMAA), C. da S. Loja – Zona Industriale, 85050 Tito Scalo, Potenza, Italy

³Karlsruher Institut für Technologie (KIT) – IMK-IFU, Kreuzeckbahnstraße 19, 82467 Garmisch-Partenkirchen, Germany

⁴Deutscher Wetterdienst, Meteorological Observatory Hohenpeissenberg, Dept. Research and Development, Albin-Schwaiger-Weg 10, 82383 Hohenpeissenberg, Germany

Received: 27 February 2014 – Accepted: 3 March 2014 – Published: 13 March 2014

Correspondence to: M. Wiegner (m.wiegner@lmu.de)

Published by Copernicus Publications on behalf of the European Geosciences Union.

Title Page

Abstract

Introduction

Conclusions

References

Tables

Figures

◀

▶

Back

Close

Full Screen / Esc

Printer-friendly Version

Interactive Discussion



Abstract

With the establishment of ceilometer networks by national weather services a discussion commenced to which extent these simple backscatter lidars can be used for aerosol research. Though primarily designed for the detection of clouds it was shown
5 that at least observations of the vertical structure of the boundary layer might be possible. However, an assessment of the potential of ceilometers for the quantitative retrieval of aerosol properties is still missing. In this paper we discuss different retrieval methods to derive the aerosol backscatter coefficient β_p with special focus on the calibration of the ceilometers. Different options based on forward and backward integration methods
10 are compared with respect to their accuracy and applicability. It is shown, that advanced lidar systems as being operated in the framework of EARLINET are excellent tools for the calibration, so that aerosol retrievals based on forward integration can readily be implemented. Furthermore, we discuss uncertainties introduced by incomplete overlap, the unknown lidar ratio, and water vapor absorption. The latter is relevant for the very
15 large number of ceilometers operating in the spectral range around $\lambda = 905$ nm. Nevertheless, the retrieval of β_p with an relative error in the order of 10 % seems feasible, so ceilometer networks can provide useful information to fill the spatial gaps between sophisticated lidar systems. As a consequence several international projects are underway to harmonize data sets from different ceilometer and lidar networks for the sake
20 of providing near real time information for weather prediction and air quality issues.

1 Introduction

Benefit of Ceilometers

M. Wiegner et al.

[Title Page](#)

[Abstract](#)

[Introduction](#)

[Conclusions](#)

[References](#)

[Tables](#)

[Figures](#)

[|◀](#)

[▶|](#)

[◀](#)

[▶](#)

[Back](#)

[Close](#)

[Full Screen / Esc](#)

[Printer-friendly Version](#)

[Interactive Discussion](#)



time and space but also a social and economical significance. Recent examples of the dramatic impact of exceptional aerosol concentrations were the eruption of the Icelandic volcano Eyjafjallajökull in 2010, (e.g., Schumann et al., 2011; Wiegner et al., 2012), leading to a temporary closure of airspace, or episodes of extreme pollution from anthropogenic (e.g., in January 2013 in Beijing, China, see <http://aqicn.org/map/>) or natural sources (e.g., Thorsteinsson et al., 2012) with severe health risks.

As a consequence improvements of measurement techniques and chemistry transport models are urgently needed. On the one hand research activities are indispensable, e.g. to improve our understanding of interactions of aerosols and clouds, and to develop advanced remote sensing techniques for the assessment of optical and microphysical aerosol properties. On the other hand, infrastructures must be implemented to monitor aerosols with high spatial and temporal coverage in near real time, e.g. ground based networks or satellite sensors.

It is undoubtedly that lidars must be the backbone of the measurement infrastructure as only they can provide quantitative range resolved aerosol parameters. With an increasing number of wavelengths and polarimetric channels lidars allow a better and more accurate characterization of optical and microphysical properties of particles. Whereas the detection of aerosol layers and their vertical extent requires only simple single-wavelength backscatter lidars, the derivation of extinction coefficient profiles and a series of intensive aerosol properties requires advanced multi-wavelength systems as high spectral resolution lidars (Shipley et al., 1983) or Raman lidars (Ansmann et al., 1992). As a consequence of the complexity of these systems they are quite expensive and thus their number is limited, and many of them are operated by research institutes only occasionally or during dedicated field campaigns.

By the end of the 1990's the need of coordinated measurements to increase the density of information was realized. As a consequence the "European aerosol research lidar network" EARLINET (Pappalardo et al., 2014) was established. Currently, a standardized procedure for the data evaluation is developed. From EARLINET Raman lidar data, aerosol backscatter β_p and extinction coefficients α_p can be retrieved

Benefit of Ceilometers

M. Wiegner et al.

Title Page

Abstract

Introduction

Conclusions

References

Tables

Figures

◀

▶

◀

▶

Back

Close

Full Screen / Esc

Printer-friendly Version

Interactive Discussion



independently, typically at two wavelengths (532 nm and 355 nm). In the near infrared (1064 nm) only β_p can be derived. The particle linear depolarization ratio δ_p (typically at one wavelength) is derived from many lidars providing information on the shape of the particles. Thus, together with the lidar ratio S_p and Angström exponents κ three intensive properties of aerosols are available that turned out to be very useful for the discrimination of different aerosol types (“aerosol typing”) (e.g., Groß et al., 2011, 2013; Wiegner et al., 2011). On the basis of this parameter set it is – under favorable conditions – possible to estimate aerosol microphysics, e.g. the refractive index and/or the effective radius of the particles (Müller et al., 1999). It was demonstrated for the Eyjafjallajökull plume that even the mass concentration of aerosol can be estimated if high quality lidar and photometer data are evaluated (e.g., Gasteiger et al., 2011), however, the uncertainty is large.

Though the potential of advanced lidars to characterize aerosol particles in detail is unsurpassed, in particular the problem of the sparse spatial sampling remains unsolved – even in case of a network such as EARLINET. The typical distance between the EARLINET stations is in the order of several hundreds of kilometers, and only a gradual increase of the number of stations is expected. Moreover, regular measurements of EARLINET are only performed on Mondays and Thursdays for a few hours; only in exceptional cases observations are performed continuously over a limited period (see Pappalardo et al., 2013). Even if in the future more continuous observations and near real time data will be available form EARLINET, the spatial issue remains because it is not sustainable to have advanced lidar systems “everywhere”.

Since several national weather services have build up networks of ceilometers, a discussion of the potential of these instruments to solve this problem came up. Ceilometers are single-wavelength, eye-safe backscatter lidars. Operational and maintenance costs are quite low. They are easy to operate and data are available in near real time. Originally, they were designed to determine cloud base heights only, but with recent improvements of the hardware, several studies have attempted to retrieve information about aerosols as well.

Benefit of Ceilometers

M. Wiegner et al.

[Title Page](#)

[Abstract](#)

[Introduction](#)

[Conclusions](#)

[References](#)

[Tables](#)

[Figures](#)

[|◀](#)

[▶|](#)

[◀](#)

[▶](#)

[Back](#)

[Close](#)

[Full Screen / Esc](#)

[Printer-friendly Version](#)

[Interactive Discussion](#)



The large number of ceilometers is a strong motivation to investigate to what extent they can fill the gaps between advanced lidar stations and how their continuous data flow can be linked to the more or less sparse measurements of such lidars. In this context it is relevant to identify the aerosol information that can be derived quantitatively from ceilometers. In this paper we do not discuss “technical” applications, e.g., ceilometers at runways of airports for the detection of cloud ceilings or fog.

In the following section we give a short survey over the existing ceilometers, their operation and their most relevant properties. Then we demonstrate which optical properties can be derived from ceilometer signals from the theoretical point of view. In the main part of this paper we discuss how these properties can be derived under realistic conditions including the aspects of calibration, error sources, and vertical coverage. A brief overview over recent applications of ceilometers for aerosol research follows. Finally, on-going and proposed activities to better exploit the benefit of ceilometers are outlined.

2 What is a ceilometer?

We define ceilometers as single-wavelength backscatter lidars with the following characteristics: the emitted wavelength is in the near infrared between 900 nm and 1100 nm to avoid strong Rayleigh scattering, the pulse repetition rate is of the order of a few kHz, and the pulse energy of the laser is sufficiently low to allow eye safe operation. Typically, a time resolution of better than one minute and a spatial resolution in the order of 15 m up to a height of 7.5 km or 15 km is available. Ceilometers can be operated unattendedly and continuously.

A survey of ceilometer and lidar stations has recently been performed mainly in the WMO Regional Association VI region (Europe including Greenland, Near East States), and including established lidar networks in North America (MPLnet) and Asia (AD-net). The survey (as of January 2014) now comprises about 1945 ceilometers and 144 lidar stations. The gathered information is stored in a data base which

Benefit of Ceilometers

M. Wiegner et al.

[Title Page](#)

[Abstract](#)

[Introduction](#)

[Conclusions](#)

[References](#)

[Tables](#)

[Figures](#)

[|◀](#)

[▶|](#)

[◀](#)

[▶](#)

[Back](#)

[Close](#)

[Full Screen / Esc](#)

[Printer-friendly Version](#)

[Interactive Discussion](#)



contains the geographical position of the instruments together with meta data information (responsible institution, instrument model, calibration method, data format). The data is visualized on a dedicated web page hosted by Deutscher Wetterdienst (<http://www.dwd.de/ceilomap>). Embedded links guide the user to quick looks (time-height cross sections) of attenuated backscatter and range-corrected (uncalibrated) backscatter signals, and station home pages. Currently, quick looks are provided by about 125 stations worldwide, most of them with a time delay of a few minutes only, i.e., in near real time. The ceilometer map and show cases for Saharan dust and volcanic ash events over Europe are available for download as Google Earth animations at the web site.

There are about 15 different instrument models in use but most of the ceilometers are from Vaisala (90 % of all installed systems, operating at a wavelength of 905 nm except the LD-40 model which operates at 855 nm), Jenoptik (1064 nm) and Eliasson (905 nm). The majority of ceilometers is operated by National Meteorological and Hydrological Services (NMHS) as part of national meteorological measurement programs. The primary output parameter is the cloud base height, which may be available for several cloud layers (e.g., Martucci et al., 2010). Other national ceilometer networks are operated by aviation control entities; these instruments are located close to airports. The two instrument models CT25K and CL31 (both from Vaisala) are widely used in Europe and the US (only CL31) while the Eliasson CBME80 is operated by Belgocontrol (Belgium) and the Swedish Meteorological and Hydrological Institute. The Jenoptik CHM15k is operated by Deutscher Wetterdienst (DWD) and the UK Meteorological Office. The Jenoptik CHM15k and the Vaisala CL51 are recently developed instruments which are more powerful than the widespread CT25K or CL31 instruments. Instrumental raw data is archived by several European NMHS and NOAA which is essential for upcoming, more sophisticated retrievals of e.g. the aerosol backscatter coefficient. For such retrievals, however, a series of prerequisite must be fulfilled, in particular the problem of calibration of the ceilometer must be solved.

Benefit of Ceilometers

M. Wiegner et al.

[Title Page](#)

[Abstract](#)

[Introduction](#)

[Conclusions](#)

[References](#)

[Tables](#)

[Figures](#)

[|◀](#)

[▶|](#)

[◀](#)

[▶](#)

[Back](#)

[Close](#)

[Full Screen / Esc](#)

[Printer-friendly Version](#)

[Interactive Discussion](#)



3 Aerosol properties from ceilometers

The basics of lidar inversion schemes for aerosol optical properties are the same for (high performance) research lidars and ceilometers. They are directly linked to backscatter and extinction of radiation. This is clear from the lidar equation (1) that describes how the received signal P depends on atmospheric parameters and range z :

$$P(z) = C_L \frac{\beta(z)}{z^2} \exp \left\{ -2 \int_0^z \alpha(z') dz' \right\} \quad (1)$$

System characteristics are described by C_L . The backscatter coefficient β and the extinction coefficient α can be split into contributions of particles and molecules, i.e.,

$$\beta = \beta_p + \beta_m \quad (2)$$

and

$$\alpha = \alpha_p + \alpha_m \quad (3)$$

By formulating Eq. (1) we implicitly consider elastic backscattering and assume that only single scattering (at range z , in most cases equivalent to "height") occurs. The wavelength can be omitted in these equations.

The solution of the lidar equation with respect to either β_p or α_p is well established and known as the Klett or Fernald solution (e.g., Fernald et al., 1972; Klett, 1981). Under typical atmospheric conditions the β_p -retrieval is more accurate, in particular in cases of low aerosol concentration and/or long wavelengths, as under these conditions the retrieved β_p -profile is less sensitive to errors of the assumed lidar ratio than the α_p -profile.

A basic assumption of the solution is that the contributions α_m and β_m can be calculated from air density profiles (e.g. from radio sonde ascents). The solution requires

Benefit of Ceilometers

M. Wiegner et al.

Title Page

Abstract

Introduction

Conclusions

References

Tables

Figures

◀

▶

◀

▶

Back

Close

Full Screen / Esc

Printer-friendly Version

Interactive Discussion



Benefit of Ceilometers

M. Wiegner et al.

[Title Page](#)[Abstract](#)[Introduction](#)[Conclusions](#)[References](#)[Tables](#)[Figures](#)[|◀](#)[▶|](#)[◀](#)[▶](#)[Back](#)[Close](#)[Full Screen / Esc](#)[Printer-friendly Version](#)[Interactive Discussion](#)

the assumption of a so called lidar ratio ($S_p = \alpha_p/\beta_p$) and of a boundary value at a reference height z_0 ($\alpha_p(z_0)$ or $\beta_p(z_0)$, respectively). The lidar ratio might be height dependent in particular if aerosol layers of different source regions are present, consequently, a reliable estimate is complicated; a problem inherent to all single wavelength lidars.

- 5 In addition, the lidar ratio at 1064 nm cannot be determined from Raman lidars, so that one has to rely on model calculations or on coincident closure experiments. The boundary value is typically determined by means of the so called Rayleigh calibration, i.e., the boundary value is set to zero. This kind of calibration can only be performed if the signal to noise ratio from aerosol free regions (e.g., the upper troposphere) is sufficiently large.
- 10 This might be challenging in case of ceilometers. As a consequence, alternative approaches to determine β_p have been investigated. This issue is discussed in detail below.

From these general remarks we can conclude that there is only one aerosol property that might be derived quantitatively from ceilometer measurements: $\beta_p(z)$. No other optical property can be derived: retrievals of α_p and δ_p fail because the required detection channels are missing (Raman scattering, depolarization). Consequently, the optical depth τ_p of an aerosol layer cannot be determined. The integrated (particle) backscatter I_p

$$I_p = \int_{z_{\text{bottom}}}^{z_{\text{top}}} \beta_p(z) \, dz \quad (4)$$

can only serve as a proxy for τ_p , as the lidar ratio is unknown. The retrieval of microphysical properties is obviously impossible, as no multi-wavelength information is available.

According to their intended use ceilometers were initially only exploited for cloud base determination (e.g., Eberhard, 1987; Robinson and McKay, 1989; Pal et al., 1992). The detection of clouds is easy and can be directly derived from the signal.

This becomes evident when we rearrange the lidar equation.

$$\frac{P(z)z^2}{C_L} = \beta^*(z) = \beta(z) \exp \left\{ -2 \int_0^z \alpha(z') dz' \right\} \quad (5)$$

Here, $\beta^*(z)$ is the attenuated backscatter. In the near infrared spectral region the transmission term is close to unity and only gradually decreasing with height. As a consequence, any pronounced change of $\beta(z)^*$ can be attributed to β . Moreover, as β_m is proportional to the air density (a “smooth” function), any significant feature of the measured profile can be attributed to β_p as well. From Eq. (5) it is obvious that layer detection is possible from calibrated and non-calibrated signals. As a consequence, the most obvious and widely used ceilometer application with respect to aerosols is the derivation of the mixing layer height z_{ml} (often synonymously used with planetary boundary layer height PBL) from the signal “shape”. This information is quite useful for weather and air quality issues, but is not considered as “optical property”.

4 Retrieval of the backscatter coefficient

As mentioned above the only optical property of aerosols that might be derived from ceilometer data is the backscatter coefficient β_p as a function of height (and time). To assess the benefit of ceilometers we have to determine under which conditions it is possible to invert the lidar equation for β_p .

4.1 Analytical solution

First, approaches to calibrate the ceilometer signals are discussed. As pointed out in Sect. 3 this is one prerequisite to derive β_p -profiles. It is worthwhile to start with a few general aspects.

Title Page

Abstract

Introduction

Conclusions

References

Tables

Figures

|◀

▶|

◀

▶

Back

Close

Full Screen / Esc

Printer-friendly Version

Interactive Discussion



The result of the Klett solution with respect to β_p can be written as follows:

$$\beta_p(z) = \frac{Z(z)}{N(z)} - \beta_m(z) \quad (6)$$

with

$$Z(z) = z^2 P(z) \exp \left\{ -2 \int_0^z [S_p(z') - S_m] \beta_m dz' \right\} \quad (7)$$

$N(z)$ can either be written in terms of the lidar constant C_L and the range-integration is performed in forward direction (from the lidar)

$$N(z) = C_L - 2 \int_0^z Z(z') dz' \quad (8)$$

or in terms of a reference value $\beta_p(z_0)$ and backward integration (towards the lidar)

$$N(z) = \frac{z_0^2 P(z_0)}{\beta_m(z_0) + \beta_p(z_0)} + 2 \int_z^{z_0} S_p(z') Z(z') dz' \quad (9)$$

It was shown by Wiegner and Geiß (2012) that the lower limit of the integral in Eq. (8) can be changed from 0 to z_{ovl} , i.e. the range of full overlap, when z_{ovl} is small and a wavelength in the infrared is used. The accuracy of this approach strongly depends on z_{ovl} and is discussed in Sect. 6.1 in more detail. The reference value in Eq. (9) is typically set to a height z_0 where no aerosols are present.

It is common to refer to the two options as the forward and the backward approach, respectively. Which of the approaches is best for a certain data set depends on the

Title Page

Abstract

Introduction

Conclusions

References

Tables

Figures

◀

▶

◀

▶

Back

Close

Full Screen / Esc

Printer-friendly Version

Interactive Discussion



Benefit of Ceilometers

M. Wiegner et al.

[Title Page](#)[Abstract](#)[Introduction](#)[Conclusions](#)[References](#)[Tables](#)[Figures](#)[|◀](#)[▶|](#)[Back](#)[Close](#)[Full Screen / Esc](#)[Printer-friendly Version](#)[Interactive Discussion](#)

type of the ceilometer, on the meteorological situation and on the availability of auxiliary data.

The forward approach is suitable for ceilometers with known C_L and long term stability. However, ceilometers are usually delivered with proprietary software that provides a “backscatter profile” with unknown correction functions accounting for incomplete overlap and unknown scaling factors for automatic adjustments, but not C_L . The backward solution, often referred to as Rayleigh calibration, is the standard approach for most research aerosol lidars at wavelengths in the UV or visible spectral range, however, this techniques frequently fails in case of ceilometers as they are not sensitive enough to detect the molecular return.

In many cases ancillary information is required for the forward or backward approaches, or is used to reduce uncertainties. On the one hand this information can be provided by co-located measurements of optical radiometers (typically a sun photometer) or advanced lidar systems (Raman lidar or high spectral resolution lidar), on the other hand special observation setups can be exploited, e.g. horizontal measurements or cloud returns. In case of different sampling, e.g. comparisons of day and night measurements or comparisons of columnar and range-resolved values, the consequences on the accuracy must be carefully assessed.

In the following section a short critical review of the applicability of these approaches for ceilometer measurements is provided.

4.2 Inversion

4.2.1 Forward approach

The basic idea of this approach is simple. If the aerosol properties α_p and β_p are known, the lidar constant C_L can be calculated from the measurement $P(z)$ according to a slightly rearranged Eq. (1), and from any $z \geq z_{\text{ovl}}$ according to

$$C_L = \frac{P(z) z^2}{\beta(z)} \frac{1}{T_{\text{ovl}}^2} \exp \left\{ 2 \int_{z_{\text{ovl}}}^z \alpha(z') dz' \right\} \quad (10)$$

with

$$T_{\text{ovl}} = \exp \left\{ - \int_0^{z_{\text{ovl}}} \alpha(z') dz' \right\} \quad (11)$$

If the extinction coefficient and the overlap range are sufficiently small the transmission T_{ovl} (Eq. 11) normally is set to 1; a qualitative discussion of this statement can be found in Porter et al. (2000). For a quantitative analysis let us consider an idealized model atmosphere with a β_p -profile at 1064 nm as indicated in Fig. 1. The lidar ratio is set to $S_p = 50$ sr. Assuming typical conditions for Munich (Central Europe) with an Angström exponent of $\kappa = 1.45$ and $\tau_p = 0.17$ at 500 nm, we define a “clear” and “turbid” case when $\tau_p = 0.085$ and $\tau_p = 0.34$ at 500 nm, respectively. Note, that the Rayleigh contribution is very small ($\beta_m \approx 8.8 \times 10^{-5} \text{ km}^{-1} \text{ sr}^{-1}$ close to the ground). For z_{ovl} we select 0.15 km and 0.6 km. In Table 1 the transmission T_{ovl} , which is unknown under realistic conditions, is listed. An estimated transmission, T_{ovl}^* ,

$$(T_{\text{ovl}})^* = \exp \{ -z_{\text{ovl}} \alpha_p(z_{\text{ovl}}) \} \quad (12)$$

by assuming a constant $\alpha_p = \alpha_p(z_{\text{ovl}})$ below z_{ovl} as shown by the dashed lines in Fig. 1. The estimate T_{ovl}^* is given in the fifth column.

It can be seen that for small z_{ovl} and τ_p the error contribution to the determination of C_L is indeed so small (less than 1 %), that even $T_{\text{ovl}}^2 = 1$ is acceptable. For larger extinction coefficients or larger z_{ovl} the error of this assumption is still below 3 %, but can be reduced to less than 1 %, if $(T_{\text{ovl}}^*)^2$ is used as an approximation of T_{ovl}^2 (rightmost

Benefit of Ceilometers

M. Wiegner et al.

[Title Page](#)

[Abstract](#)

[Introduction](#)

[Conclusions](#)

[References](#)

[Tables](#)

[Figures](#)

[◀](#)

[▶](#)

[◀](#)

[▶](#)

[Back](#)

[Close](#)

[Full Screen / Esc](#)

[Printer-friendly Version](#)

[Interactive Discussion](#)



Benefit of Ceilometers

M. Wiegner et al.

[Title Page](#)[Abstract](#)[Introduction](#)[Conclusions](#)[References](#)[Tables](#)[Figures](#)[|◀](#)[▶|](#)[◀](#)[▶](#)[Back](#)[Close](#)[Full Screen / Esc](#)[Printer-friendly Version](#)[Interactive Discussion](#)

column). Only for ceilometers with large z_{ovl} (e.g., 0.6 km) and turbid conditions, the error of C_L becomes significant with an underestimate of almost 7 % if the transmission term is set to 1. If, however, the unknown transmission in the overlap region is estimated by assuming a constant extinction (a common assumption), the underestimate can be reduced to 1 %. Though even larger τ_p might occur, and the vertical profile of α_p might deviate from the assumed decrease, we conclude that the accuracy of C_L is not a critical issue, when a correction as described in Eq. (12) is applied.

If the system parameters of the ceilometer are constant in time or if changes can reliably be tracked, β_p can be derived at any time as shown by Eqs. (6) to (8). As shown above the inherent error of C_L can be assumed to be less than 1 %. Additional errors are introduced by errors of α and β according to Eq. (10).

Wiegner and Geiß (2012) proposed a methodology based on the provision of α_p and β_p from the combination of selected ceilometer measurements at night time when Rayleigh calibration was possible (up to 2 h averages). Co-located sun photometer measurements of τ_p were used to constrain S_p in the Klett algorithm. The approach was applied only when the time difference between the ceilometer and the sun photometer observations was below 2 to 3 h and when the variability of the aerosol distribution was low, mainly in cloud-free time periods and close to sunset or sunrise. Their algorithm was applied to Jenoptik CHM15kx measurements and accounts for intentional changes of the system's sensitivity with background radiation (i.e., changes of C_L). From an extensive error calculation an overall uncertainty of less than 10 % was found. As a result β_p can be retrieved with a temporal resolution of a few minutes, and thus can easily be used for near real time applications.

An alternative methodology makes use of co-located and coincident measurements with a high performance multi-wavelength Raman lidar as available within EARLINET as proposed by Wiegner (2010). If measurements at the same wavelength are available the ratio of the signals (lidar and ceilometer) directly provides the ratio of the respective lidar constants $C = C_{L,1}/C_{L,2}$. Then, the Klett backward solution is applied to the data of the advanced lidar system. With a carefully estimated lidar ratio and

Rayleigh calibration, α_p and β_p can be determined and consequently – according to Eq. (10) – $C_{L,1}$ of the advanced lidar. With the above mentioned factor C the lidar constant of the ceilometer $C_{L,2}$ can be retrieved easily. A multi-wavelength Raman lidar is advantageous because it provides $\beta_p(z)$ at infrared wavelengths with comparatively high accuracy as the spectral behavior of the aerosol optical properties can be taken into account (Pappalardo et al., 2010) (see also Sect. 5.1). Examples from EARLINET measurements of the LMU show that this procedure can be applied, even if the two instruments are separated by 25 km. This is possible as the terrain around Munich is quite flat and no significant local aerosol sources exist, conditions that are certainly not valid for every location. An example of such a comparison (signals averaged over 20 min) is shown in Fig. 2: the lidar and the ceilometer are located in Maisach and Munich, respectively. It is obvious that small differences in the profiles exist though the overall agreement is excellent. As a result, the normalization factor C slightly depends on the range where the two signals are matched. This additional uncertainty in the determination of lidar constant of the ceilometer can be avoided if the instruments are co-located.

The main advantage of the forward approach is that co-located and coincident reference measurements are required only for a limited number of cases: they could be from a Raman lidar, a high-spectral resolution lidar or a sun photometer. The disadvantage is that the stability of the ceilometer must be monitored to account for a possible degradation of the detector or the laser. This variability of C_L can be accounted for by periodical re-calibration.

In this context, we briefly want to mention a very special approach proposed by O'Connor et al. (2004). It relies on measuring the path integrated $\beta^*(z)$ in a fully attenuating stratocumulus cloud. It was shown that the integrated $\beta^*(z)$ is equal to the reciprocal of twice the lidar ratio and the multiple scattering factor η (Platt, 1979), provided that these parameters are range independent. In cases when S_p and η of the cloud are known the ceilometer data can be scaled until the integrated backscatter

Benefit of Ceilometers

M. Wiegner et al.

[Title Page](#)

[Abstract](#)

[Introduction](#)

[Conclusions](#)

[References](#)

[Tables](#)

[Figures](#)

[|◀](#)

[▶|](#)

[◀](#)

[▶](#)

[Back](#)

[Close](#)

[Full Screen / Esc](#)

[Printer-friendly Version](#)

[Interactive Discussion](#)



agrees with the theoretical value. As a consequence, C_L has been assessed. Accurate calibration within 10 % relative uncertainty can be achieved according to the authors.

This approach was successfully applied by Stachlewska et al. (2010) when they used returns from low-level cumulus clouds in the Arctic that did not saturate the ceilometer signals. In general, however, this approach might be challenging for ceilometers as their sensitivity is optimized for aerosol backscattering (e.g., detection of the boundary layer top) and cirrus clouds and thus, the strong return from low liquid water clouds might saturate the detector. Furthermore, if the penetration depth of the ceilometer signal is only a few range bins and the dynamical range of the signal is extremely large, the exploitation of the signal is critical. The unknown multiple scattering factors further limit the accuracy of the calibration. Even if these problems can be solved the procedure is certainly time consuming.

4.2.2 Backward approach

Ceilometers are typically working in a spectral region where the molecular scattering is weak. This, combined with the low pulse energy of ceilometers the detection of molecular signals is per se very difficult. Thus, significant temporal averaging over time periods that depend on the signal to noise ratio (SNR) of the ceilometer data is mandatory to perform a Rayleigh calibration. However, the low SNR might introduce quite high statistical uncertainties of the β_p -retrieval, and not detected spurious aerosol loading could introduce a bias.

A two-step approach based on the Rayleigh calibration was proposed by Binietoglou et al. (2011). This inversion technique is based on the idea that the above mentioned problem can be overcome by integrating the ceilometer signals over a quite long period, up to 8 h. Such an integration improves the SNR, consequently allowing the detection of molecular signals at typically aerosol-free altitudes – say 6 km – even during daytime. In the first step of the algorithm the signals of the selected long period are averaged and a Klett backward inversion is performed thus obtaining a “reference” backscatter coefficient profile. The selected period must be per definitionem cloud free at the

Benefit of Ceilometers

M. Wiegner et al.

Title Page

Abstract

Introduction

Conclusions

References

Tables

Figures

◀

▶

Back

Close

Full Screen / Esc

Printer-friendly Version

Interactive Discussion



calibration altitude, but aerosol layers at lower altitudes do not need to be stable in time. In the second step, the Klett inversion is performed with a higher temporal resolution, using the reference profile to estimate a calibration value at a lower altitude, even if aerosols are present. Binietoglou et al. (2011) compared their retrieval with β_p -profiles derived from the multi-wavelength lidar PEARL (Potenza EARLINET Raman lidar) and the agreement for the selected few cases looks promising but needs more investigations.

Several authors (e.g., Heese et al., 2010; Wiegner and Geiß, 2012) have confirmed that for the Rayleigh calibration several hours of cloud free conditions are required: for the Jenoptik CHM15kx, averages over 2 to 3 h are required for night and day time measurements, respectively. For Vaisala's CL51 ceilometer similar conclusions hold. This is a limitation that, depending on the region, can be rather restrictive. It should be emphasized that any kind of Rayleigh calibration fails in the presence of low or mid-level clouds.

A common attempt to overcome the inherent problems of the backward Klett solution is the use of the aerosol optical depth τ_p from co-located sun photometer measurements, see e.g., Flentje et al. (2010) or Heese et al. (2010). In this approach, the β_p -retrieval from the ceilometer measurements must be converted into a α_p -profile assuming a certain lidar ratio. The two parameters required for the backward approach, S_p and $\beta_{p,\text{ref}}$, can be iterated until integration of α_p yields the aerosol optical depth received from the photometer. In case of night time measurements, τ_p is interpolated from the previous and/or following day. In this case, the stability of the atmospheric stratification must be confirmed by adequate measurements; inspection of time-height cross sections of range corrected ceilometer signals might be sufficient in most cases: in particular the advection of elevated layers (e.g. Saharan dust) can be detected by this approach. The potential of star or lunar photometers (Barretou et al., 2013) has not yet been exploited to overcome the “night time problem”.

To avoid assumptions of the aerosol optical depth during night time Heese et al. (2010) used the wavelength independent extinction of cirrus clouds provided by

Benefit of Ceilometers

M. Wiegner et al.

[Title Page](#)

[Abstract](#)

[Introduction](#)

[Conclusions](#)

[References](#)

[Tables](#)

[Figures](#)

[|◀](#)

[▶|](#)

[◀](#)

[▶](#)

[Back](#)

[Close](#)

[Full Screen / Esc](#)

[Printer-friendly Version](#)

[Interactive Discussion](#)



Benefit of Ceilometers

M. Wiegner et al.

[Title Page](#)[Abstract](#)[Introduction](#)[Conclusions](#)[References](#)[Tables](#)[Figures](#)[|◀](#)[▶|](#)[◀](#)[▶](#)[Back](#)[Close](#)[Full Screen / Esc](#)[Printer-friendly Version](#)[Interactive Discussion](#)

co-incident lidar measurements to estimate a boundary value and assumed a standard lidar ratio.

Another basic problem arises from the region of incomplete overlap of the ceilometer. With increasing height, the agreement between the optical depths suffers from the unknown τ_p of the missing layer. To reduce this problem ground based measurements of extinction coefficients might help to refine τ_p of these layers. Flentje et al. (2010) used nephelometer measurements for this purpose, consequently additional assumptions are required to estimate extinction coefficient, and to extrapolate to the ceilometer wavelength (Porter et al., 2000). If no auxiliary measurements are available a vertically constant α_p is assumed within the overlap region, cf. Eq. (12).

All of these strategies are quite time consuming and can hardly be automated, as for each measurement a special treatment of the data and an optimized combination of auxiliary data and assumptions is required. Thus in case of ceilometers, the backward solution includes a number of serious shortcomings and limitations, all of them are based on the very low SNR at the far end of the measurement range.

5 Discussion

5.1 The lidar ratio issue

From Sect. 3 we know that the knowledge of the lidar ratio is essential for solving the lidar equation. This problem is relevant for backscatter lidars and ceilometers, and wrong estimates affect ceilometers in the same way as backscatter lidars.

Though it is generally assumed that the systematic error of β_p is “small” when a wrong S_p is used, we again want to discuss this issue in more detail. For the forward solution the influence of S_p on the function $Z(z)$ in Eq. (7) is obvious. For $N(z)$ it is more complex as the lower limit of the integral is zero (Eq. 8). Thus, we split the integral into two terms and get

$$N(z) = C_L - 2 \int_0^{z_{\text{ovl}}} Z(z') dz' - 2 \int_{z_{\text{ovl}}}^z Z(z') dz' \quad (13)$$

It can be shown that this equation can be replaced in very good approximation (relative error below 0.5 %, and not depending on aerosol abundance) by

$$N(z) = C_L(1 - F) - 2 \int_{z_{\text{ovl}}}^z Z(z') dz' \quad (14)$$

with

$$F := 2 \int_0^{z_{\text{ovl}}} S_p(z') \beta(z') dz' \quad (15)$$

- 10 The dependence of F , and thus also of $N(z)$, on S_p can be determined straight forward. Results for the same model parameters as shown in Fig. 1 are shown in Fig. 3. Plotted is the difference $\Delta\beta_p$ of the retrieved and the true (i.e. the model input) values for clear and turbid conditions, and when the lidar ratio is underestimated ($S_p = 40 \text{ sr}$) or overestimated ($S_p = 60 \text{ sr}$) by 10 sr. Full lines relate to the forward approach, dashed lines to the backward approach. In case of the forward approach two lines each are plotted according to the different overlap heights z_{ovl} . It can be seen that the magnitude of the uncertainty introduced by wrong S_p -estimates is of the same order of magnitude for the forward and backward approach, but the height dependence is different. They are in the order of $\Delta\beta_p < 1 \times 10^{-5} \text{ km}^{-1} \text{ sr}^{-1}$ for the clear case and $\Delta\beta_p < 5 \times 10^{-4} \text{ km}^{-1} \text{ sr}^{-1}$ for the turbid case with the exception of the lowermost atmosphere, when the backward approach is used. This corresponds to relative errors below 3 % in the clear case and 10 % in the turbid case. A closer look reveals that, if the forward approach is used, the

deviation slightly increases with increasing z_{owl} only if the lidar ratio is underestimated. In case of an overestimate the accuracy of the retrieved β_p is reduced for ceilometers with low overlap. This unexpected result is a consequence of compensating effects.

We conclude that though the influence of a wrong S_p -assumption on $\beta_p(z)$ is typically small, the best possible estimate should be used. Direct measurements of S_p at 1064 nm are however virtually not available: HSRL measurements are not known to the authors, and Raman lidars only provide S_p at 532 nm and/or 355 nm, thus, spectral extrapolation is required. The calculations of S_p at 1064 nm from scattering theory is no realistic alternative: to be consistent with theory

$$S_p = \frac{1}{\omega_0 p(\pi)} \quad (16)$$

where ω_0 is the single scattering albedo and $p(\pi)$ the phase function (normalized to 1) for backward scattering, S_p requires the knowledge of the size distribution, the refractive index and the shape of the particles. Markowicz et al. (2008) tried to estimate S_p by inverting multi-spectral measurements of a nephelometer, or to prescribe the phase function by means of the Henyey–Greenstein phase function with an assumed asymmetry parameter. However, these approaches suffer from large uncertainties, and require resources that are normally not available. As a consequence, a set of aerosol types has been defined, and S_p of the most likely aerosol type is used.

20 5.2 Water vapor absorption

As already mentioned most Vaisala ceilometers nominally emit radiation at 905 nm. In fact, as the laser is not temperature stabilized, the emitted wavelength varies by a few nanometers and the effective emitted spectrum typically has a width of about 3 nm. Furthermore, differences between individual ceilometers might occur. This wavelength range is influenced by water vapor absorption, which is not the case at 1064 nm. As a consequence, the ceilometer signal is influenced by the (highly variably) atmospheric water vapor distribution at the time of the measurement, and Eq. (3) must be replaced

by

$$\alpha = \alpha_p + \alpha_m + \alpha_w \quad (17)$$

where α_w is the range dependent water vapor (volume) absorption coefficient. To correct for the water vapor effect it is required to know the vertical distribution of the absolute humidity (or an equivalent quantity), the spectral absorption coefficients of water vapor and the spectrum of the laser. Typically, the latter is unknown for a given measurement. The water vapor distribution can be derived from sophisticated lidars (DIAL or Raman), numerical models, or from radiosonde ascents, i.e., from temperature and relative humidity profiles, often with limited accuracy and poor vertical resolution. If no radiosonde data are available one has to rely on standard profiles and integrated values such as precipitable water w , certainly a critical approach in view of the large spatiotemporal variability of water vapor.

If water vapor absorption takes place Eq. (7) must be replaced by

$$Z(z) = z^2 P(z) \exp \left\{ -2 \int_0^z [(S_p - S_m) \beta_m - \alpha_w] dz' \right\} \quad (18)$$

A case study of the water vapor effect on signals of Vaisala's CT25k-ceilometer was presented by Markowicz et al. (2008), but under operational conditions such a detailed consideration of water vapor absorption is not possible. Sundström et al. (2009) also encountered the absorption problem when evaluation CL31 measurements. To illustrate the influence of water vapor on the ceilometer signal and the consequences for aerosol retrievals a small numerical study may help. The aerosol distribution introduced in Sect. 4.2.1 (Fig. 1) is assumed, the water vapor distribution is described in terms of relative humidity f and set to either 0 % or 99 % for certain height ranges, and p and T profiles according to the US standard atmosphere is used. To investigate the water vapor absorption effect separately, we assume that the aerosol is hydrophobic. It is

Benefit of Ceilometers

M. Wiegner et al.

[Title Page](#)

[Abstract](#)

[Introduction](#)

[Conclusions](#)

[References](#)

[Tables](#)

[Figures](#)

[|◀](#)

[▶|](#)

[◀](#)

[▶](#)

[Back](#)

[Close](#)

[Full Screen / Esc](#)

[Printer-friendly Version](#)

[Interactive Discussion](#)



Benefit of Ceilometers

M. Wiegner et al.

[Title Page](#)

[Abstract](#)

[Introduction](#)

[Conclusions](#)

[References](#)

[Tables](#)

[Figures](#)

[|◀](#)

[▶|](#)

[◀](#)

[▶](#)

[Back](#)

[Close](#)

[Full Screen / Esc](#)

[Printer-friendly Version](#)

[Interactive Discussion](#)



Benefit of Ceilometers

M. Wiegner et al.

[Title Page](#)[Abstract](#)[Introduction](#)[Conclusions](#)[References](#)[Tables](#)[Figures](#)[|◀](#)[▶|](#)[◀](#)[▶](#)[Back](#)[Close](#)[Full Screen / Esc](#)[Printer-friendly Version](#)[Interactive Discussion](#)

depends on the selected lidar ratio S_p , however, this effect is in most cases smaller than the effect due to the neglected water vapor.

Note, that for spectral ranges with stronger water vapor absorption, e.g. 905–910 nm, the errors are larger, up to 35 %. Errors also increase, if w is larger, e.g. in tropical atmospheres, or if there is undetected water vapor in the Rayleigh fit range.

As a conclusion it is mandatory to consider water vapor absorption when aerosol optical properties are to be retrieved from ceilometer measurements in the spectral region around 905 nm. The degree to which the error can be reduced by using water vapor profiles derived from radio sonde ascents, calculated from relative humidity and temperature, can only be estimated as it depends on the temporal and spatial difference of the ceilometer measurement and the radio sonde launch, the total water vapor content, the vertical resolution of the water vapor profile, and the emitted spectrum of the laser.

For demonstration, let us assume a height-independent relative uncertainty of the absolute humidity of 20 %, and an effective absorption coefficient $\alpha_w(z)$ estimated from the weighted water vapor transmission $T_{w,\text{eff}}$ according to Eq. (19)

$$T_{w,\text{eff}}^2(z) = \frac{\sum_{i=1}^N w_i T_w^2(\lambda_i, z)}{\sum_{i=1}^N w_i} = \exp \left\{ -2 \int_0^z \alpha_w(z') dz' \right\} \quad (19)$$

Here, λ_i is a set of representative wavelengths in the spectral range of the laser, and w_i the according weights. Then, $\alpha_w(z)$ as required for Eq. (18) can be determined and the backward algorithm can be used to retrieve β_p . We have applied this approach to the first two examples of Fig. 5 (case III and case IV, clear) with an under- and an overestimate of α_w of 20 %, respectively. The same uncertainty of the lidar ratios S_p as above is assumed. The results are shown in Fig. 6 in terms of the ratio of the retrieved and the correct β_p . It can be seen that the error of β_p is considerably reduced to less than 5 % compared to 10 % and 20 % before (see Fig. 5).

6 The measurement range

The measurement range of a ceilometer is essential for various reasons. A trivial reason is that the benefit of aerosol information increases with the vertical coverage; in particular the lowest layers of the troposphere are of interest as most of the aerosols 5 reside there and the most direct impact on life is close to the ground. A second reason is, the better the coverage of the lower most atmosphere the better is the fulfilment of the requirements of the inversion according to Eq. (8), see Wiegner and Geiß (2012). The coverage of the free troposphere is required for the Rayleigh calibration.

6.1 The near end

10 The lower limit of the measurement range is – as already demonstrated – a crucial point for the applicability of the forward approach as shown in Eq. (11), and for the consequences of the uncertainty of the assumed lidar ratio, see Eq. (15).

Typically the minimum height of ceilometer derived β_p -profiles is between approximately 200 m (e.g., CHM15kx, CL51) and 1000 m (CHM15k). To extend the measurement range towards the ground, overlap correction functions can be applied; they are either provided by the manufacturer or must be determined by the user. In case of the 15 CHM15k, Jenoptik provides overlap correction functions down to approximately 500 m. In case of Vaisala ceilometers, the output profiles are already corrected for incomplete overlap, but the function itself is unknown to the user and cannot be modified.

20 Two approaches are common to determine an overlap correction function: it can be determined from horizontal measurements or from intercomparison with lidars/ceilometers of known overlap characteristics. The first option requires horizontally homogeneous conditions with respect to α and β (no local aerosol sources, no isolated dynamical systems, no orographical structures) and a ceilometer that may be operated 25 in horizontal orientation. The constant extinction coefficient α_0 can be derived from the derivative of the logarithm of the range corrected signal (Eq. 20)

AMTD

7, 2491–2543, 2014

Title Page

Abstract

Introduction

Conclusions

References

Tables

Figures

◀

▶

◀

▶

Back

Close

Full Screen / Esc

Printer-friendly Version

Interactive Discussion



$$\frac{d}{dz} \left(\ln P(z) z^2 \right) = -2 \alpha_0 \quad (20)$$

Then, the “overlap function” $O(z)$ of the ceilometer can be determined as the ratio of the measured signal and the idealized signal according to the lidar equation (Eq. 1)

- 5 and the constant α_0 . Figure 7 shows an example based on horizontal measurements of a Vaisala CL51 ceilometer on 5 March 2013 in Garmisch-Partenkirchen. Each curve represents averages over 30 min, the mean overlap function is shown as the black line.
- 10 To ensure that only homogeneous atmospheric situations are considered, averages are only used if the temporal variability of α_0 is below 4 % between 0.3 km and 0.5 km, and below 10 % between 0.5 km and 1.0 km. Then, the latter α_0 is used for the full range to determine the hypothetical signal of the ceilometer without overlap effects. In spite of the large variability of the calculated $O(z)$ our findings suggest that the signal in general is overestimated between 0.06 km and 0.5 km. Below the signals are rapidly changing and not trustworthy. As mentioned the data of CL51 ceilometers undergoes
- 15 an internal overlap correction by the vendor software. Our results suggest, that this correction is overcompensating the incomplete overlap. Thus, if the data are used “as is”, the ceilometer measurements tends to pretend an elevated aerosol layer above 0.045 km.

- 20 It should be mentioned that the requirement of horizontal homogeneity of the atmosphere is often hard to fulfill. Measurements at the center of Munich were found to be absolutely unsuitable, and even at Garmisch-Partenkirchen adequate situations were rare. Thus, a very careful selection of the measurement site and time is mandatory.

- 25 The second option requires a reference system with the same wavelength. Here, sophisticated lidars can be very useful if dedicated near field telescopes are available or scanning of the line of sight is possible. Then, the overlap function can be derived from the signal ratio of the ceilometer and the reference system.

In principle, ceilometers of well known overlap characteristics might also be used as reference. In this context, the relevance of comparing profiles at the same wavelength

Benefit of Ceilometers

M. Wiegner et al.

[Title Page](#)

[Abstract](#)

[Introduction](#)

[Conclusions](#)

[References](#)

[Tables](#)

[Figures](#)

◀

▶

◀

▶

[Back](#)

[Close](#)

[Full Screen / Esc](#)

[Printer-friendly Version](#)

[Interactive Discussion](#)



shall be emphasized, that means, that comparisons of Jenoptik and Vaisala ceilometers can be doubtful. One obvious reason is the influence of water vapor absorption (see Sect. 5.2) but even under dry conditions there are intrinsic problems. This can be demonstrated by a comparison of coincident and co-located Jenoptik CHM15kx (1064 nm) and Vaisala CL51 (905 nm) measurements. Figure 8 shows a comparison from 26 March 2012 in Munich; profiles are averaged over 30 min. The signal of the Vaisala ceilometer is scaled in such a way that both range corrected signals match between an altitude of 1.1 km and 1.5 km. It can be seen that the signals in the mixing layer are almost identical down to about 0.5 km. If an overlap correction according to Fig. 7 is applied to the CL51 ceilometer, the agreement is extended to approximately 0.25 km. The perfect agreement between 0.25 km and 1.7 km not only indicates similar performance of both ceilometers to sound the PBL, but is also an independent test of $O(z)$ as derived from horizontal measurements. Below approximately 0.2 km, ceilometer signals should not be used.

Above the mixing layer the disagreement of the signals is primarily due to the wavelength dependence of β_p , and the fact, that the free troposphere is almost free of aerosols. Considering wavelengths at 905 nm and 1064 nm and a typical Angström exponent of $\kappa=1.45$, the aerosol backscatter coefficient is expected to be approximately 30 % larger at the shorter wavelength. Thus, if the signals are matched above the mixing layer no overlap function $O(z)$ can be derived because the ratio of the signals predominantly depends on aerosol properties and no on the optical design.

6.2 The far end

The far end of the measurement range is in particular relevant if the backward solution including the Rayleigh calibration shall be applied (see Sect. 4.2.2). During night time and in case of low optical depth of the boundary layer this might be possible when integration in the order of one to two hours is possible. In all other cases it is quite unlikely, however, general conclusions are difficult. Thus, to determine the measurement range of ceilometers, comparisons with simultaneous and co-located lidar observations

Benefit of Ceilometers

M. Wiegner et al.

[Title Page](#)

[Abstract](#)

[Introduction](#)

[Conclusions](#)

[References](#)

[Tables](#)

[Figures](#)

[|◀](#)

[▶|](#)

[◀](#)

[▶](#)

[Back](#)

[Close](#)

[Full Screen / Esc](#)

[Printer-friendly Version](#)

[Interactive Discussion](#)



Benefit of Ceilometers

M. Wiegner et al.

[Title Page](#)

[Abstract](#)

[Introduction](#)

[Conclusions](#)

[References](#)

[Tables](#)

[Figures](#)

[|◀](#)

[▶|](#)

[◀](#)

[▶](#)

[Back](#)

[Close](#)

[Full Screen / Esc](#)

[Printer-friendly Version](#)

[Interactive Discussion](#)



3.2 km. This uppermost layer is detected by none of the ceilometers. The extended layer, with $\tau_p = 0.15$ at 355 nm as derived from Raman measurements, is clearly visible in the CHM15k signals whereas only traces can be detected by the CT25k due to the strong attenuation of the lower atmosphere. Thus, elevated aerosol layers might be completely or partly missed by CT25k measurements.

Limitations of the measurement range of the ceilometers also plays a role with respect to the detection of cirrus clouds. Again, one example may illustrate the performance (Fig. 11): here we compare the Jenoptik CHM15kx and the Vaisala CL51 ceilometer, observations are from 18 January 2012 and took place in Munich. It can be seen that extended ice clouds are resolved in a similar way by both ceilometers, with a slightly better performance of the CHM15kx in the uppermost parts of the cloud.

7 Applications

It has been shown in the previous sections that the derivation of optical properties of aerosols is restricted to the particle backscatter coefficient β_p . As already mentioned 15 ceilometer data are, however, of use even in cases when no quantitative evaluation of optical properties is possible (e.g., Emeis et al., 2007). A few examples are briefly discussed in the following.

7.1 Aerosol layer detection

Aerosol layer presence and extension can be determined from uncalibrated ceilometer data, e.g., in many cases it is sufficient to analyze the range corrected signal or 20 $\beta^*(r, t)$. As the top of the mixing layer z_{ml} is correlated with a (significant) reduction of backscattering, most algorithms are based on the investigation of the signal slope. Different algorithms are known from the literature (e.g., Melfi et al., 1985; Menut et al., 1999; Davis et al., 2000; Brooks, 2003). Elevated layers can be identified in a similar 25 way. This has primarily been demonstrated for lidar measurements, e.g. Morille et al.

Benefit of Ceilometers

M. Wiegner et al.

Title Page

Abstract

Introduction

Conclusions

References

Tables

Figures

◀

▶

◀

▶

Back

Close

Full Screen / Esc

Printer-friendly Version

Interactive Discussion



(2007) or Baars et al. (2008), however, the underlying concepts can be applied for ceilometer data as well. As a consequence, z_{ml} is included into the output data sets of most commercial ceilometers. However, details of the algorithms are not published, in particular, the treatment of signals that suffer from incomplete overlap remains unclear, and typically no adjustments can be made by the user.

An example of retrieved z_{ml} is shown in Fig. 12, based on CHM15kx data of 12 July 2013 at Munich. Two methods are compared: the blue line marks the results from the STRAT algorithm (Morille et al., 2007), the red line is based on a hybrid algorithm that primarily aims at the determination of the convective boundary layer. The latter is a combination of methods for edge detection (e.g. wavelet covariance transform, gradient method, variance method) and edge tracking to increase the reliability of the layer detection and attribution. It is obvious that both retrievals in general show very good agreement with what is expected from visual inspection; note, that normally the visual impression is taken as reference because “the truth” is unknown. However, the example also reveals the inherent problems of these retrievals: layers are often well identified but the attribution to atmospheric features is per se difficult and not unambiguous. Between 07:00 UTC and 10:00 UTC the STRAT-result “jumps” between the convective boundary layer and the residual layer. During night time the mixing layer shows several internal layers that sometimes leads to problems in the attribution (before 06:00 UTC).

To assess the aerosol profiling capabilities of the CHM15k ceilometer in a more general sense we use observations from MUSA (multi-wavelength system for aerosol) lidar during 2010 at CIAO as reference, and calculate the percentage of elevated layers that were also detected by the CHM15k. The numbers were determined for day and night time separately, and derived from visual inspection of time height cross sections of $P r^2$. Figure 13 shows that the percentage of detection gradually decrease from 100 % for layers below 1.5 km, to 50 % for layers below 3.7 km, and to zero at about 5 km if night time measurements are considered. During daytime, when separated layers are higher in altitude due to the larger extent of the mixing layer, the percentage of detection is lower than 50 % at 1.8 km, and drops to zero for layers above approximately 3.5 km.

Benefit of Ceilometers

M. Wiegner et al.

[Title Page](#)

[Abstract](#)

[Introduction](#)

[Conclusions](#)

[References](#)

[Tables](#)

[Figures](#)

[|◀](#)

[▶|](#)

[◀](#)

[▶](#)

[Back](#)

[Close](#)

[Full Screen / Esc](#)

[Printer-friendly Version](#)

[Interactive Discussion](#)



Tough it is clear that the detection of an elevated layer does not only depend on the optical depth of that layer but also on the transmission below (Mona et al., 2009), this comparison shows that ceilometers can certainly contribute useful data to climatologies of Z_{ml} and statistics of the occurrence of elevated layers, though within certain limits.

5 7.2 Validation of chemistry transport models

In the previous section it was demonstrated that in particular mixing layer heights can be determined from ceilometer data. This outcome can e.g. be used for the validation of different convection parameterizations in chemistry transport models; the need became obvious e.g. by the second GABLS experiment (Svensson et al., 2011). The 10 following simulations were carried out with WRF/Chem (Grell et al., 2005) for three nested domains with horizontal resolutions of 36 km, 9 km, and 2.25 km. Two different parameterizations are compared: the YSU (Yonsei University) planetary boundary layer scheme (Hong et al., 2006) and the Mellor–Yamada–Janjic (MYJ) scheme (Janjic, 2002). The YSU-scheme is a first order K-closure scheme with an additional parameterized countergradient term in the eddy-diffusion equation for considering non-local 15 transport. For daytime convective boundary layers, the criterion for the boundary layer height is that the virtual potential temperature Θ_v is 1 K larger than Θ_v of the lowest layer. The criterion for the stable PBL is based on the bulk Richardson number Ri of the lowermost layer. The PBL-height is that height, where Ri exceeds the critical Richardson 20 number, which is assumed to have a value of 0.25 in WRF version 3 (Hong and Kim, 2008). The MYJ-scheme uses the 1.5-order (level 2.5) turbulence closure model of Mellor and Yamada (1982). This scheme solves among others the equation for the turbulent kinetic energy (TKE). The PBL-height is diagnosed as the height where the TKE drops below $0.1 \text{ m}^2 \text{ s}^{-2}$.

25 For comparison the PBL-height as determined from CL31 ceilometer measurements applying the software provided by the manufacturer is used (Münkel, 2007). Shown are measurements in downtown Augsburg, Germany, of four consecutive days of July 2008 (Fig. 14). There is no consistent picture of the agreement between observations and

Benefit of Ceilometers

M. Wiegner et al.

[Title Page](#)

[Abstract](#)

[Introduction](#)

[Conclusions](#)

[References](#)

[Tables](#)

[Figures](#)

[◀](#)

[▶](#)

[Back](#)

[Close](#)

[Full Screen / Esc](#)

[Printer-friendly Version](#)

[Interactive Discussion](#)



model, but in general the diurnal cycles and the absolute values agree fairly. Only for 22 July the agreement is worse, i.e. the diurnal cycle is not detected by the ceilometer retrieval and z_{ml} is much lower. Furthermore, a small temporal offset between measurements and model results exists. During night time the MYJ-scheme better agrees with the ceilometer analysis than the YSU-scheme. Note, that the reasons for the differences are not evident: shortcomings of the model as well as misinterpretation of ceilometer signals with respect to the PBL-height as mentioned above might happen. Thus, Fig. 14 highlights the urgent need of improving layer detection algorithms to fully exploit the potential of ceilometers.

Ceilometer data have also been used to validate chemistry transport model simulations of elevated layers. A recent example is the Eyjafjallajökull eruption in April 2010 (Emeis et al., 2011). On the basis of ceilometer data, the validation is however restricted to the dispersion of the volcanic ash plume, more detailed information as the optical depth or the mass concentration is not available. Under favorable conditions it should only be possible to derive the integrated backscatter I_p (Eq. 4) of aerosol layers. The validation of modeled aerosol optical depth is thus not possible with ceilometer data; I_p can however be used as a test for plausibility.

It is certainly worthwhile to extend such studies to dust transport forecasts as provided in the framework of the WMO Sand and Dust Storm Warning Advisory and Assessment System (SDS-WAS), e.g. the vertical distribution of dust as provided by the DREAM model (Nickovic et al., 2001).

8 Summary and conclusions

With the advent of lidar remote sensing techniques our knowledge with respect to aerosols has been improved significantly: not only the spatiotemporal distribution of aerosols could be determined but also the derivation of optical properties became feasible. In particular EARLINET, a science driven programme, succeeded to develop adequate lidar technologies, measurement strategies, and data processing tools, thus

Benefit of Ceilometers

M. Wiegner et al.

[Title Page](#)

[Abstract](#)

[Introduction](#)

[Conclusions](#)

[References](#)

[Tables](#)

[Figures](#)

◀

▶

◀

▶

[Back](#)

[Close](#)

[Full Screen / Esc](#)

[Printer-friendly Version](#)

[Interactive Discussion](#)



demonstrating the feasibility of quantitative aerosol characterization. However, costs for investment and maintenance of advanced lidar systems are prohibitive for establishing dense networks that are required to cover the spatial scales of the aerosol variability. As a consequence, it is worthwhile to investigate to which extent the recently established ceilometer networks can provide added value to EARLINET type aerosol remote sensing.

It was shown in this paper that the retrieval of the aerosol backscatter coefficient β_p from ceilometer measurements is possible, however, a careful calibration is required. A promising strategy is the application of the Klett forward algorithm. The main advantage is, that – in contrast to the Klett backward inversion – calibration is required only occasionally and it is not affected by the (very) low SNR in the upper troposphere. It was emphasized that the retrieval of aerosol properties are prone to considerable errors if the ceilometer operates at wavelength with water vapor absorption (905 nm). Incomplete overlap is not a severe issue at typical ceilometer wavelengths, nevertheless corrections should be applied if available. The uncertainties introduced by wrong lidar ratios are inherent for any backscatter lidar.

Ceilometer measurements can benefit from EARLINET lidar primarily with respect to calibration issues. The advantage is that strictly coincident and co-located measurements are possible, even and in particular during night, when the signal-to-noise ratio of the ceilometer is best. Then, the lidar constant C_L of the ceilometer can be determined with the best possible accuracy. If furthermore water vapor absorption can be excluded (e.g., at 1064 nm) the uncertainty of the retrieved β_p should remain below 10 %. A generally applicable accuracy cannot be given as it depends on the ceilometer type and the meteorological condition. It is expected that profiles of β_p can be provided with a height resolution of a few tens of meters and a temporal resolution better than one minute.

It should be emphasized that ceilometer data, even if they are not calibrated, are useful. They can provide information of the aerosol stratification, e.g. mixing layer height or the extent of elevated layers. Such information can be used to understand qualitatively

Benefit of Ceilometers

M. Wiegner et al.

[Title Page](#)

[Abstract](#)

[Introduction](#)

[Conclusions](#)

[References](#)

[Tables](#)

[Figures](#)

[|◀](#)

[▶|](#)

[◀](#)

[▶](#)

[Back](#)

[Close](#)

[Full Screen / Esc](#)

[Printer-friendly Version](#)

[Interactive Discussion](#)



Benefit of Ceilometers

M. Wiegner et al.

[Title Page](#)[Abstract](#)[Introduction](#)[Conclusions](#)[References](#)[Tables](#)[Figures](#)[|◀](#)[▶|](#)[◀](#)[▶](#)[Back](#)[Close](#)[Full Screen / Esc](#)[Printer-friendly Version](#)[Interactive Discussion](#)

References

Benefit of Ceilometers

M. Wiegner et al.

[Title Page](#)

[Abstract](#)

[Introduction](#)

[Conclusions](#)

[References](#)

[Tables](#)

[Figures](#)

[◀](#)

[▶](#)

[◀](#)

[▶](#)

[Back](#)

[Close](#)

[Full Screen / Esc](#)

[Printer-friendly Version](#)

[Interactive Discussion](#)



Benefit of Ceilometers

M. Wiegner et al.

Title Page

Abstract

Introduction

Conclusions

References

Tables

Figures

◀

▶

◀

▶

Back

Close

Full Screen / Esc

Printer-friendly Version

Interactive Discussion



Davis, K. J., Gamage, N., Hagelberg, C. R., Kiemle, C., Lenschow, D. H., and Sullivan, P. P.: An objective method for deriving atmospheric structure from airborne lidar observations, *J. Atmos. Ocean. Tech.*, 17, 1455–1468, 2000. 2517

Eberhard, W. L.: Cloud signals from lidar and rotating beam ceilometers compared with pilot ceiling, *J. Atmos. Ocean. Tech.*, 3, 499–512, 1987. 2498

5 Emeis, S., Jahn, C., Münkel, C., Münsterer, C., and Schäfer, K.: Multiple atmospheric layering and mixing-layer height in the Inn valley observed by remote sensing, *Meteorol. Z.*, 16, 415–424, doi:10.1127/0941-2948/2007/0203, 2007. 2517

10 Emeis, S., Forkel, R., Junkermann, W., Schäfer, K., Flentje, H., Gilge, S., Fricke, W., Wiegner, M., Freudenthaler, V., Groß, S., Ries, L., Meinhardt, F., Birmili, W., Münkel, C., Obleitner, F., and Suppan, P.: Measurement and simulation of the 16/17 April 2010 Eyjafjallajökull volcanic ash layer dispersion in the northern Alpine region, *Atmos. Chem. Phys.*, 11, 2689–2701, doi:10.5194/acp-11-2689-2011, 2011. 2520

15 Fernald, F. G., Herman, B. M., and Reagan, J. A.: Determination of aerosol height distributions by lidar, *J. Appl. Meteorol.*, 11, 482–489, 1972. 2497

Flentje, H., Claude, H., Elste, T., Gilge, S., Köhler, U., Plass-Dülmer, C., Steinbrecht, W., Thomas, W., Werner, A., and Fricke, W.: The Eyjafjallajökull eruption in April 2010 – detection of volcanic plume using in-situ measurements, ozone sondes and lidar-ceilometer profiles, *Atmos. Chem. Phys.*, 10, 10085–10092, doi:10.5194/acp-10-10085-2010, 2010. 2506, 2507

20 Gasteiger, J., Groß, S., Freudenthaler, V., and Wiegner, M.: Volcanic ash from Iceland over Munich: mass concentration retrieved from ground-based remote sensing measurements, *Atmos. Chem. Phys.*, 11, 2209–2223, doi:10.5194/acp-11-2209-2011, 2011. 2494

Grell, G. A., Peckham, S. E., Schmitz, R., McKeen, S. A., Frost, G., Skamarock, W. C., and Eder, B.: Fully coupled “online” chemistry within the WRF model, *Atmos. Environ.*, 39, 6957–6975, 2005. 2519

25 Groß, S., Tesche, M., Freudenthaler, V., Toledano, C., Wiegner, M., Ansmann, A., Althausen, D., and Seefeldner, M.: Characterization of Saharan dust, marine aerosols and mixtures of biomass burning aerosols and dust by means of multi-wavelength depolarization- and Raman-measurements during SAMUM-2, *Tellus B*, 63, 706–724, doi:10.1111/j.1600-0889.2011.00556.x, 2011. 2494

30 Groß, S., Esselborn, M., Weinzierl, B., Wirth, M., Fix, A., and Petzold, A.: Aerosol classification by airborne high spectral resolution lidar observations, *Atmos. Chem. Phys.*, 13, 2487–2505, doi:10.5194/acp-13-2487-2013, 2013. 2494

- Heese, B., Flentje, H., Althausen, D., Ansmann, A., and Frey, S.: Ceilometer lidar comparison: backscatter coefficient retrieval and signal-to-noise ratio determination, *Atmos. Meas. Tech.*, 3, 1763–1770, doi:10.5194/amt-3-1763-2010, 2010. 2506
- Hong, S.-Y. and Kim, S.-W.: Stable boundary layer mixing in a vertical diffusion scheme, Proc. Ninth Annual WRF User's Workshop, Boulder, CO, National Center for Atmospheric Research, 3.3, available at: <http://www.mmm.ucar.edu/wrf/users/workshops/WS2008/abstracts/3-03.pdf> (last access: 12 March 2014), 2008. 2519
- Hong, S.-Y., Noh, Y., and Dudhia, J.: A new vertical diffusion package with an explicit treatment of entrainment processes, *Mon. Weather Rev.*, 134, 2318–2341, 2006. 2519
- Janjic, Z. I.: Nonsingular Implementation of the Mellor – Yamada Level 2.5 Scheme in the NCEP Mesomodel, *NCEP Office Note*, 437, 61 pp., 2002. 2519
- Klett, J. D.: Stable analytical inversion solution for processing lidar returns, *Appl. Optics*, 20, 211–220, 1981. 2497
- Madonna, F., Amodeo, A., Boselli, A., Cornacchia, C., Cuomo, V., D'Amico, G., Giunta, A., Mona, L., and Pappalardo, G.: CIAO: the CNR-IMAA advanced observatory for atmospheric research, *Atmos. Meas. Tech.*, 4, 1191–1208, doi:10.5194/amt-4-1191-2011, 2011. 2516
- Markowicz, K. M., Flatau, P. J., Kardas, A. E., Remiszewska, J., Stelmaszczyk, K., and Woeste, L.: Ceilometer retrieval of the boundary layer vertical aerosol extinction structure, *J. Atmos. Ocean. Tech.*, 25, 928–944, 2008. 2509, 2510
- Martucci, G., Milroy, C., and O'Dowd, C. D.: Detection of cloud-base height using Jenoptik CHM15K and Vaisala CL31 ceilometers, *J. Atmos. Ocean. Tech.*, 27, 305–318, 2010. 2496
- Mayer, B. and Kylling, A.: Technical note: The libRadtran software package for radiative transfer calculations – description and examples of use, *Atmos. Chem. Phys.*, 5, 1855–1877, doi:10.5194/acp-5-1855-2005, 2005. 2511
- Melfi, S. H., Spinhirne, J. D., Chou, S. H., and Palm, S. P.: Lidar observation of the vertically organized convection in the planetary boundary layer over the ocean, *J. Clim. Appl. Meteor.*, 24, 806–821, 1985. 2517
- Mellor, G. L. and Yamada, T.: Development of a turbulence closure model for geophysical fluid problems, *Rev. Geophys.*, 20, 851–875, 1982. 2519
- Menut, L., Flamant, C., Pelon, J., and Flamant, P. H.: Urban boundary-layer height determination from lidar measurements over the Paris area, *Appl. Optics*, 38, 945–954, 1999. 2517
- Mona, L., Pappalardo, G., Amodeo, A., D'Amico, G., Madonna, F., Boselli, A., Giunta, A., Russo, F., and Cuomo, V.: One year of CNR-IMAA multi-wavelength Raman lidar mea-

Benefit of Ceilometers

M. Wiegner et al.

Title Page

Abstract

Introduction

Conclusions

References

Tables

Figures

|◀

▶|

◀

▶

Back

Close

Full Screen / Esc

Printer-friendly Version

Interactive Discussion



Benefit of Ceilometers

M. Wiegner et al.

[Title Page](#)[Abstract](#)[Introduction](#)[Conclusions](#)[References](#)[Tables](#)[Figures](#)[|◀](#)[▶|](#)[◀](#)[▶](#)[Back](#)[Close](#)[Full Screen / Esc](#)[Printer-friendly Version](#)[Interactive Discussion](#)

jafjallajökull volcanic cloud over Europe observed by EARLINET, *Atmos. Chem. Phys.*, 13, 4429–4450, doi:10.5194/acp-13-4429-2013, 2013. 2494, 2516

Pappalardo, G., Amodeo, A., Apituley, A., Comeron, A., Freudenthaler, V., Linné, H., Ans-
mann, A., Bösenberg, J., D'Amico, G., Mattis, I., Mona, L., Wandinger, U., Amiridis, V.,
5 Alados-Arboledas, L., Nicolae, D., and Wiegner, M.: EARLINET: towards an advanced sus-
tainable European aerosol lidar network, *Atmos. Meas. Tech. Discuss.*, in press, 2014. 2493

Platt, C. M. R.: Remote sounding of high cloud, Part I: Calculations of the visible and infrared
optical properties from lidar and radiometer measurements. *J. Appl. Meteorol.*, 18, 1130–
1143, 1979. 2504

10 Porter, J. N., Lienert, B., and Sharma, S. K.: Using horizontal and slant lidar measurements
to obtain calibrated aerosol scattering coefficients from a coastal lidar in Hawaii, *J. Atmos.
Ocean. Technol.*, 17, 1445–1454, 2000. 2502, 2507

15 Robinson, C. E. and McKay, D. J.: A practical cloud algorithm for automatic weather stations,
Instruments and Observing Report No. 35, Fourth World Meteorological Organisation Technical
Conference on Instruments and Methods of Observation, WMO/TD 303 (World Meteorological
Organisation), Geneva, 1989. 2498

Sasano, Y., Browell, E. V., and Ismail, S.: Error caused by using a constant extinction/backscattering ratio in the lidar solution, *Appl. Optics*, 24, 3929–3932, 1985.

20 Schumann, U., Weinzierl, B., Reitebuch, O., Schlager, H., Minikin, A., Forster, C., Baumann, R.,
Sailer, T., Graf, K., Mannstein, H., Voigt, C., Rahm, S., Simmet, R., Scheibe, M., Lichtenstern,
M., Stock, P., Rüba, H., Schäuble, D., Tafferner, A., Rautenhaus, M., Gerz, T., Ziereis, H., Krautstrunk,
M., Mallaun, C., Gayet, J.-F., Lieke, K., Kandler, K., Ebert, M., Weinbruch, S., Stohl, A., Gasteiger,
J., Groß, S., Freudenthaler, V., Wiegner, M., Ansmann, A., Tesche, M., Olafsson, H., and Sturm, K.: Airborne observations of the Eyjafjalla volcano ash
25 cloud over Europe during air space closure in April and May 2010, *Atmos. Chem. Phys.*, 11,
2245–2279, doi:10.5194/acp-11-2245-2011, 2011. 2493

Shipley, S. T., Tracy, D. H., Eloranta, E. W., Trauger, J. T., Sroga, J. T., Roesler, F. L., and
Weinman, J. A.: A High Spectral Resolution Lidar to measure optical scattering properties of
atmospheric aerosols, Part I: Instrumentation and theory, *Appl. Optics*, 23, 3716–3724, 1983.
30 2493

Sundström, A. M., Nousiainen, T., and Petäjä, T.: On the quantitative low-level
aerosol measurements using ceilometer-type lidar, *J. Tech.*, 26, 2340–2352,
doi:10.1175/2009JTECHA1252.1, 2009. 2510

Discussion Paper | Benefit of Ceilometers

M. Wiegner et al.

[Title Page](#)[Abstract](#)[Introduction](#)[Conclusions](#)[References](#)[Tables](#)[Figures](#)[◀](#)[▶](#)[◀](#)[▶](#)[Back](#)[Close](#)[Full Screen / Esc](#)[Printer-friendly Version](#)[Interactive Discussion](#)

Benefit of
Ceilometers

M. Wiegner et al.

Stachlewska, I. S., Markowicz, K. M., and Piadlowski, M.: On forward Klett's inversion of ceilometer signals, in: Proc. 25th ILRC International Laser Radar Conference, 5–9 July 2010, St. Petersburg, Russia, 1154–1157, 2010. 2505

Svensson, G., Holtslag, A. A. M., Kumar, V., Mauritzen, T., Steeneveld, G. J., Angevine, W. M., Bazile, E., Beljaars, A., de Bruijn, E. I. F., Cheng, A., Conangla, L., Cuxart, J., Ek, M., Falk, M. J., Freedman, F., Kitagawa, H., Larson, V. E., Lock, A., Mailhot, J., Masson, V., Park, S., Pleim, J., Söderberg, S., Weng, W., and Zampieri, M.: Evaluation of the diurnal cycle in the atmospheric boundary layer over land as represented by a variety of single-column models: the second GABLS experiment, *Bound.-Lay. Meteorol.*, 140, 177–206, doi:10.1007/s10546-011-9611-7, 2011. 2519

Takamura, T., Sasano, Y., and Hayasaka, T.: Tropospheric aerosol optical properties derived from lidar, sun photometer, and optical particle counter measurements, *Appl. Optics*, 33, 7132–7140, 1994.

Thorsteinsson, T., Jóhannsson, T., Stohl, A., and Kristiansen, N. I.: High levels of particulate matter in Iceland due to direct ash emissions by the Eyjafjallajökull eruption and resuspension of deposited ash, *J. Geophys. Res.*, 117, B00C05, doi:10.1029/2011JB008756, 2012. 2493

Wiegner, M.: Potential of ceilometers for aerosol remote sensing: a preliminary assessment, in: Proc. 25th International Laser Radar Conference, 5–9 July 2010, St. Petersburg, Russia, 914–917, 2010. 2503

Wiegner, M. and Geiß, A.: Aerosol profiling with the Jenoptik ceilometer CHM15kx, *Atmos. Meas. Tech.*, 5, 1953–1964, doi:10.5194/amt-5-1953-2012, 2012. 2500, 2503, 2506, 2513

Wiegner, M., Groß, S., Freudenthaler, V., Schnell, F., and Gasteiger, J.: The May/June 2008 Saharan dust event over Munich: intensive aerosol parameters from lidar measurements, *J. Geophys. Res.*, Vol. 116, D23213, doi:10.1029/2011JD016619, 2011. 2494

Wiegner, M., Gasteiger, J., Groß, S., Schnell, F., Freudenthaler, V., and Forkel, R.: Characterization of the Eyjafjallajökull ash-plume: potential of lidar remote sensing, *Phys. Chem. Earth*, 45–46, 79–86, doi:10.1016/j.pce.2011.01.006, 2012. 2493

Title Page

Abstract

Introduction

Conclusions

References

Tables

Figures

|◀

▶|

◀

▶

Back

Close

Full Screen / Esc

Printer-friendly Version

Interactive Discussion



Benefit of Ceilometers

M. Wiegner et al.

Table 1. Squared transmission of the overlap range T_{ovl}^2 as defined in Eq. (11) and estimate $(T_{\text{ovl}}^*)^2$ derived from extrapolation (see text for details); τ_p (at 1064 nm) is given in km^{-1} , z_{ovl} in km.

	τ_p	z_{ovl}	T_{ovl}^2	$(T_{\text{ovl}}^*)^2$	$(T_{\text{ovl}}^*/T_{\text{ovl}})^2$
CLR	0.028	0.150	0.995	0.995	1.0002
TUR	0.114	0.150	0.980	0.981	1.0010
CLR	0.028	0.600	0.982	0.985	1.0026
TUR	0.114	0.600	0.932	0.941	1.0106

[Title Page](#)

[Abstract](#)

[Introduction](#)

[Conclusions](#)

[References](#)

[Tables](#)

[Figures](#)

[|◀](#)

[▶|](#)

[◀](#)

[▶](#)

[Back](#)

[Close](#)

[Full Screen / Esc](#)

[Printer-friendly Version](#)

[Interactive Discussion](#)



Benefit of Ceilometers

M. Wiegner et al.

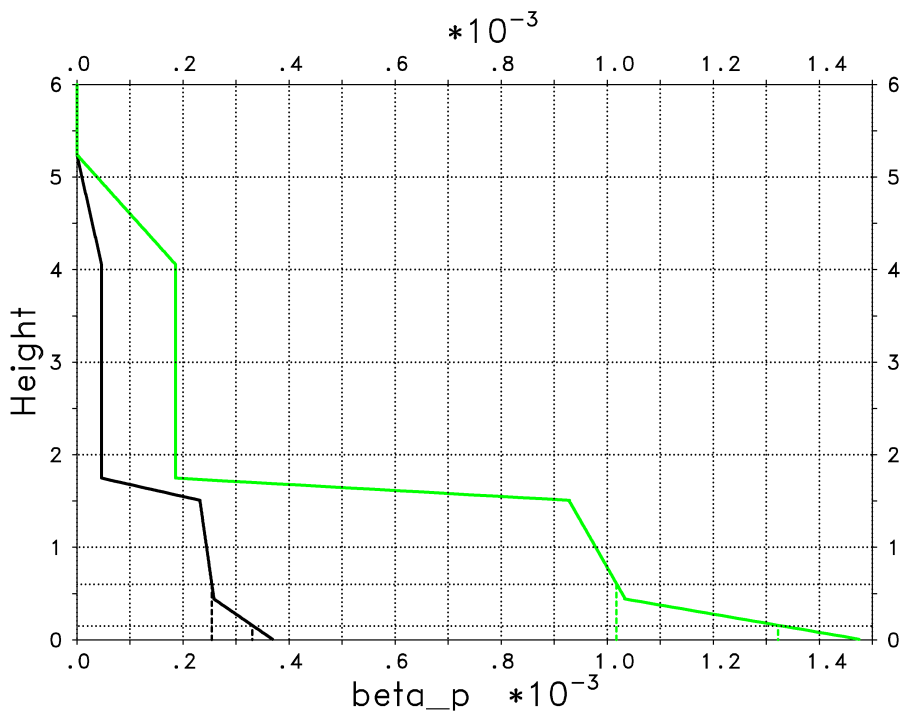


Fig. 1. Profiles of aerosol backscatter coefficient β_p (in $\text{km}^{-1} \text{sr}^{-1}$) for model calculations at 1064 nm, height is given in km. The two curves indicated clear (black) and turbid (green) conditions. The dashed lines show the extrapolation to the ground for ceilometers with $z_{\text{ovl}} = 0.6 \text{ km}$ and $z_{\text{ovl}} = 0.15 \text{ km}$, respectively.

- [Title Page](#)
- [Abstract](#) [Introduction](#)
- [Conclusions](#) [References](#)
- [Tables](#) [Figures](#)
- [◀](#) [▶](#)
- [◀](#) [▶](#)
- [Back](#) [Close](#)
- [Full Screen / Esc](#)

[Printer-friendly Version](#)[Interactive Discussion](#)

Benefit of Ceilometers

M. Wiegner et al.

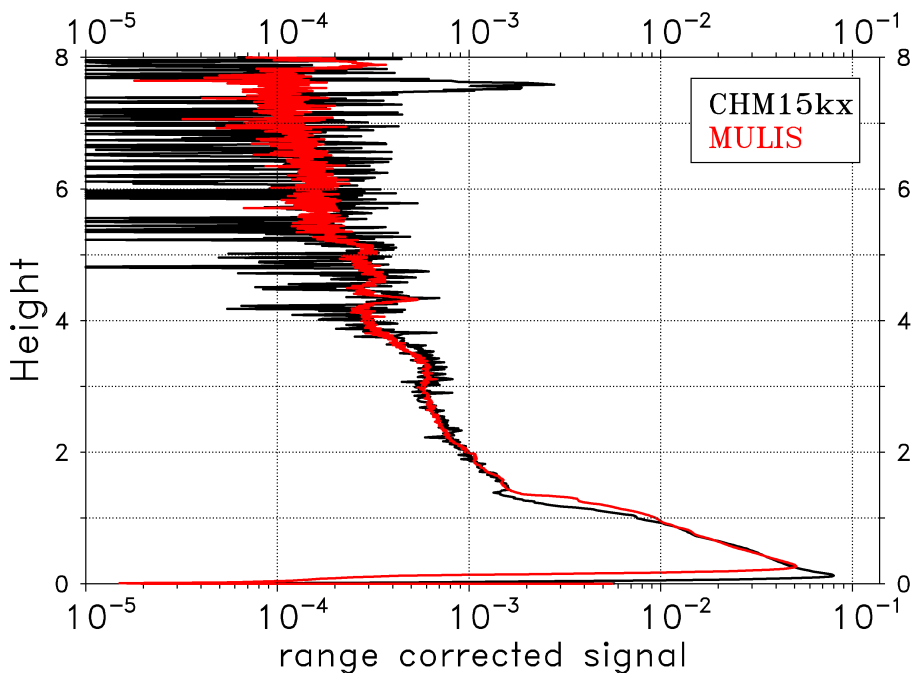


Fig. 2. Comparison of $P r^2$ at 1064 nm (in arbitrary units) of the ceilometer (CHM15kx) in Munich (black) and the EARLINET lidar (MULIS) in Maisach (red), 5 May 2011, averaged from 20:00 to 20:20 UTC. Height is given in km. The signals are normalized between 0.5 km and 1.0 km.

[Title Page](#)[Abstract](#)[Introduction](#)[Conclusions](#)[References](#)[Tables](#)[Figures](#)[◀](#)[▶](#)[Back](#)[Close](#)[Full Screen / Esc](#)[Printer-friendly Version](#)[Interactive Discussion](#)

Benefit of Ceilometers

M. Wiegner et al.

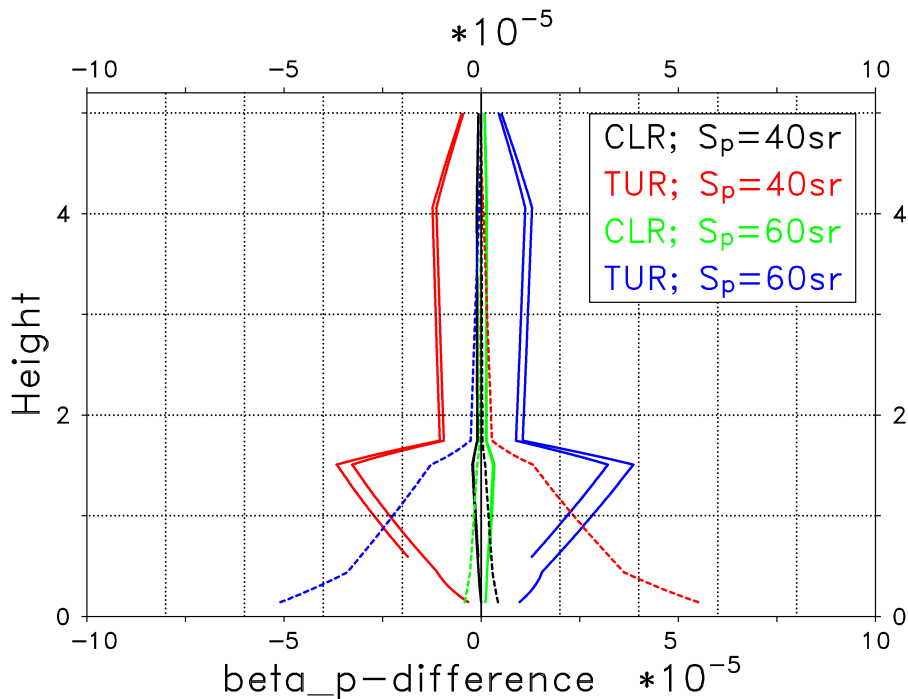


Fig. 3. Differences of the retrieved and the true β_p -profile (see Fig. 1, in $\text{km}^{-1} \text{sr}^{-1}$), when the forward (full lines) and the backward approach (dashed lines) are applied. Retrievals for clear (“CLR”) and turbid (“TUR”) situations (see Tab. 1) and different assumptions of the lidar ratio ($S_p = 40\text{sr}$ and $S_p = 60\text{sr}$) are plotted in colors as indicated. Height is given in km.

- [Title Page](#)
- [Abstract](#) [Introduction](#)
- [Conclusions](#) [References](#)
- [Tables](#) [Figures](#)
- [◀](#) [▶](#)
- [◀](#) [▶](#)
- [Back](#) [Close](#)
- [Full Screen / Esc](#)
- [Printer-friendly Version](#)
- [Interactive Discussion](#)



Benefit of Ceilometers

M. Wiegner et al.

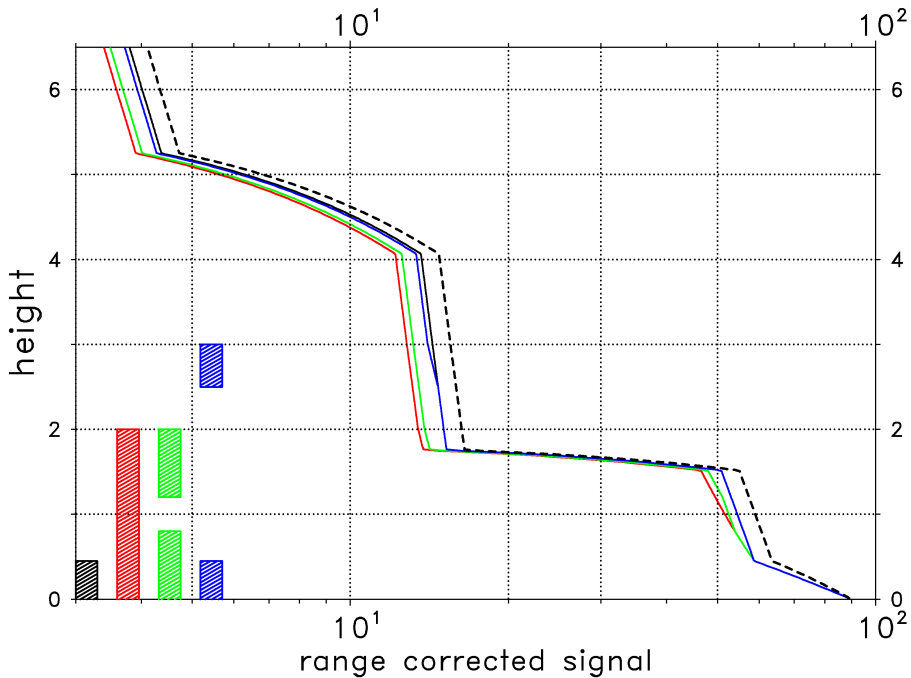


Fig. 4. Simulated range corrected ceilometer signals (in arbitrary units) at 905 nm influenced by different vertical water vapor distributions (cases I to IV): the relative humidity is set to 99 % in height ranges as indicated by the colored bars at the left corner of the figure, elsewhere it is assumed to be 0 %. The dashed line is for a dry atmosphere. As aerosol distribution the clear case shown in Fig. 1 is selected, height is given in km.

Title Page	Abstract	Introduction
Conclusions	References	
Tables	Figures	
◀	▶	
◀	▶	
Back	Close	
Full Screen / Esc		
Printer-friendly Version		
Interactive Discussion		



Benefit of Ceilometers

M. Wiegner et al.

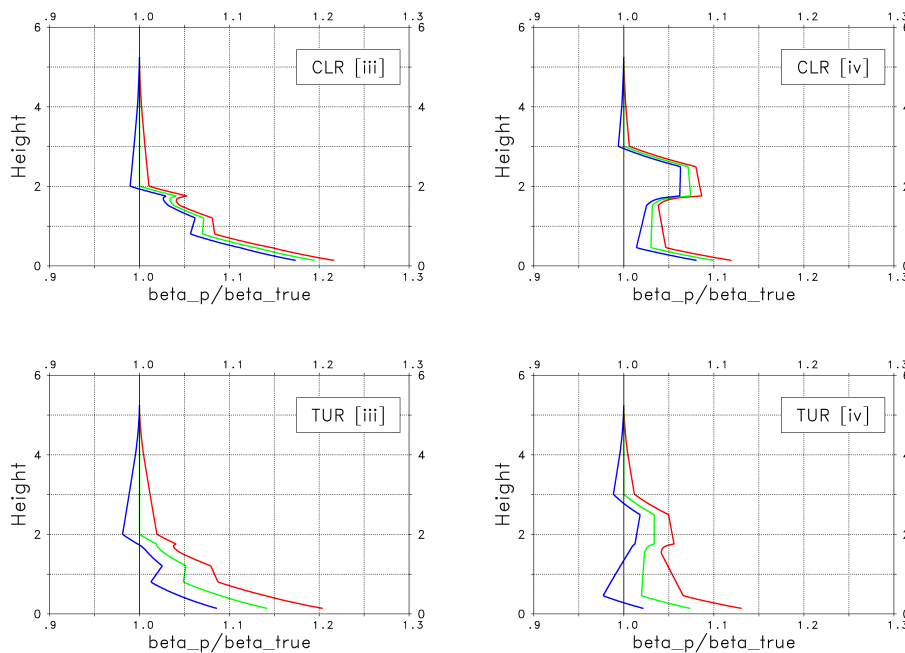


Fig. 5. Ratio of retrieved (from the backward algorithm) and the true β_p for clear (upper row) and turbid conditions (bottom) and different the water vapor distributions (case III on the left, case IV on the right). The colors indicate S_p as used in the retrieval (50 sr green, 40 sr red, 60 sr blue), height is given in km. The retrievals do not account for water vapor absorption.

Title Page	Abstract	Introduction
Conclusions	References	
Tables	Figures	
◀	▶	
◀	▶	
Back	Close	
Full Screen / Esc		
	Printer-friendly Version	
	Interactive Discussion	



Benefit of Ceilometers

M. Wiegner et al.

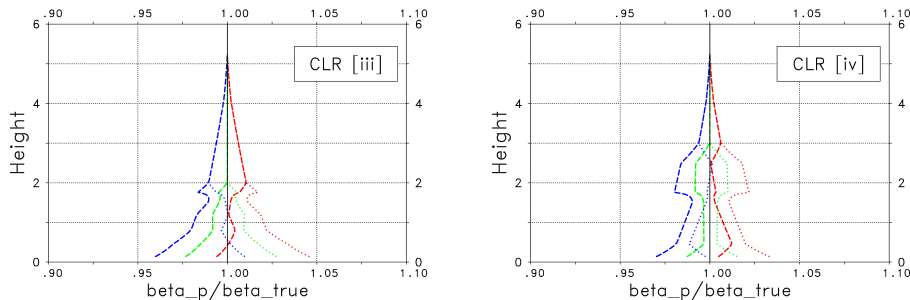


Fig. 6. Ratio of retrieved and the true β_p for clear conditions and different the water vapor distributions (left: case III, right: case IV) with an overestimate (dashed) and an underestimate (dotted) of the water vapor absorption by 20 %. The colors indicate S_p as used in the retrieval (50 sr green, 40 sr red, 60 sr blue), height is given in km.

- [Title Page](#)
- [Abstract](#) [Introduction](#)
- [Conclusions](#) [References](#)
- [Tables](#) [Figures](#)
- [◀](#) [▶](#)
- [◀](#) [▶](#)
- [Back](#) [Close](#)
- [Full Screen / Esc](#)

- [Printer-friendly Version](#)
- [Interactive Discussion](#)



Benefit of Ceilometers

M. Wiegner et al.

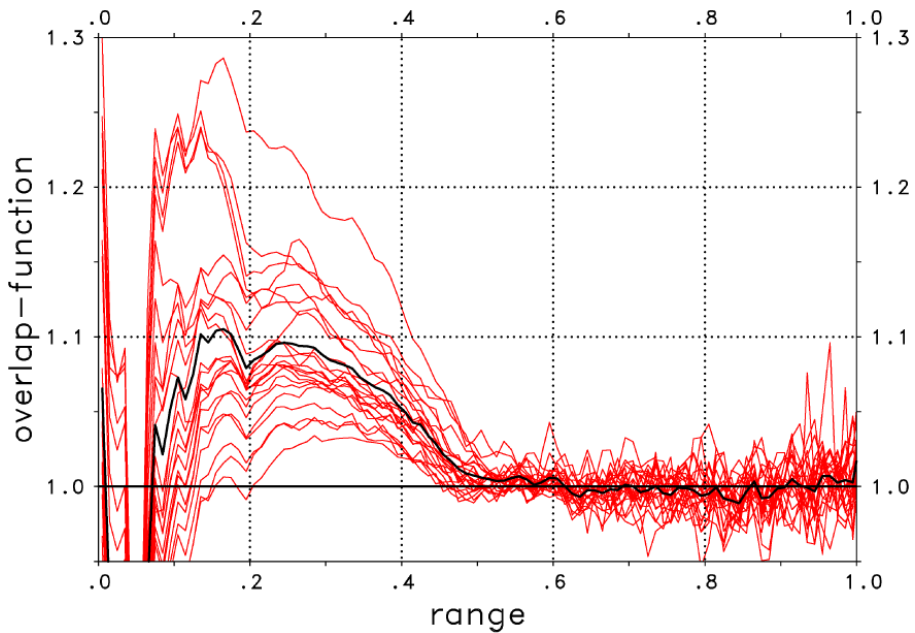


Fig. 7. Overlap function $O(z)$ as determined from horizontal measurements (Vaisala CL51 ceilometer, 5 March 2013, in Garmisch-Partenkirchen). The red lines indicate 30 min averages, the black line is the average of the individual lines. Range is given in km. For details, see text.

- [Title Page](#)
- [Abstract](#) [Introduction](#)
- [Conclusions](#) [References](#)
- [Tables](#) [Figures](#)
- [◀](#) [▶](#)
- [◀](#) [▶](#)
- [Back](#) [Close](#)
- [Full Screen / Esc](#)

- [Printer-friendly Version](#)
- [Interactive Discussion](#)



Benefit of Ceilometers

M. Wiegner et al.

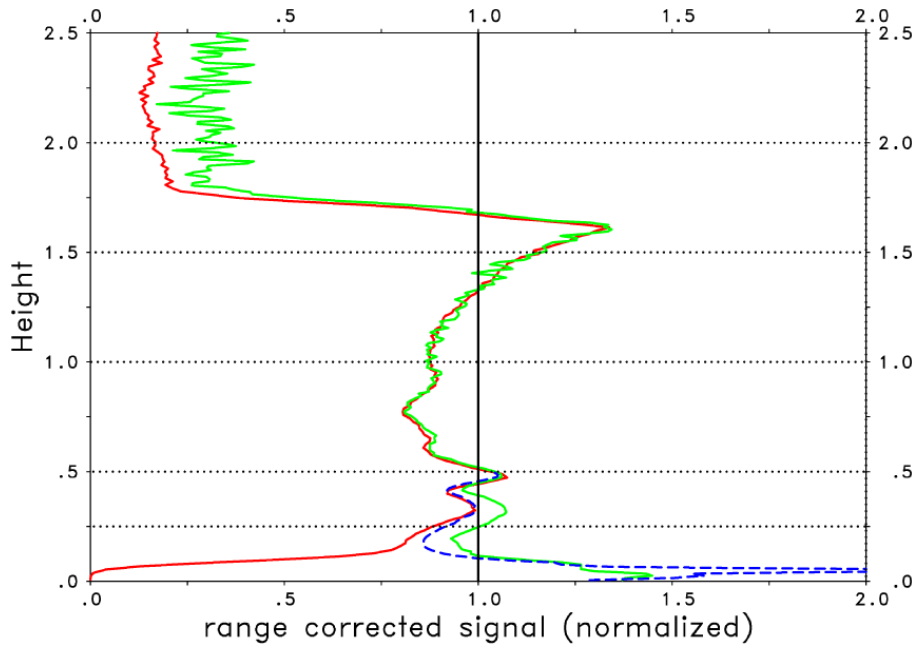


Fig. 8. Range corrected signals of a CHM15kx (red) and a CL51 ceilometer without (green) and with (blue) overlap correction from 26 March 2012, averaged from 21:00 UTC till 21:30 UTC.

- [Title Page](#)
- [Abstract](#) [Introduction](#)
- [Conclusions](#) [References](#)
- [Tables](#) [Figures](#)
- [◀](#) [▶](#)
- [◀](#) [▶](#)
- [Back](#) [Close](#)
- [Full Screen / Esc](#)
- [Printer-friendly Version](#)
- [Interactive Discussion](#)



Benefit of Ceilometers

M. Wiegner et al.

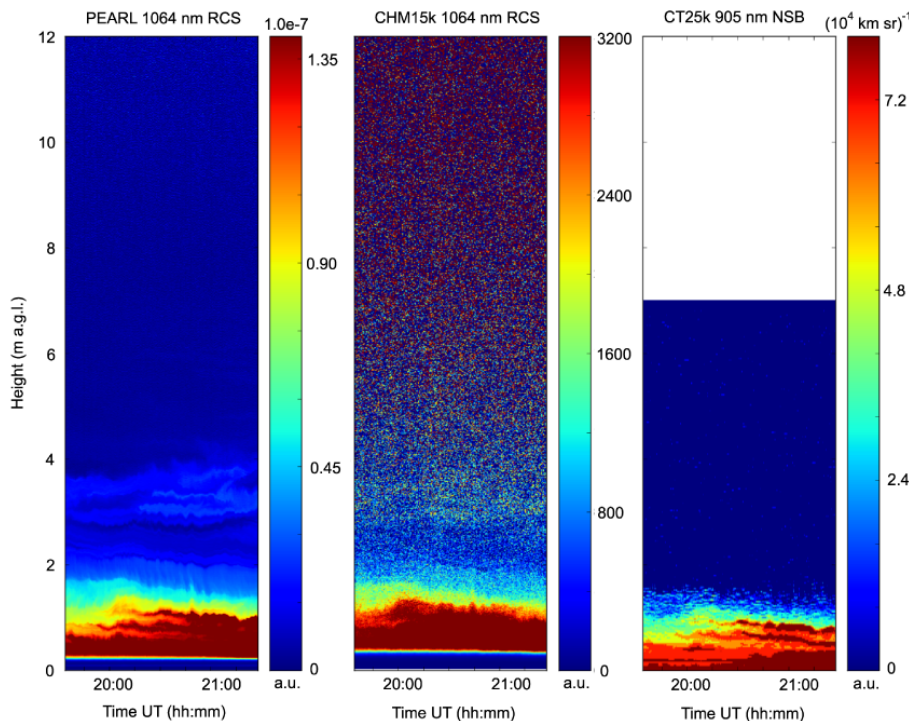


Fig. 9. Observation time series obtained with PEARL (left), CHM15k (center) and CT25K (right) on 12 July 2010 from 19:15 to 21:15 UTC: shown are range corrected signals (PEARL, CHM15k) and “normalized sensitivity backscattering” (CT25k).

Title Page	Abstract	Introduction
Conclusions	References	
Tables	Figures	
◀	▶	
◀	▶	
Back	Close	
Full Screen / Esc		

[Printer-friendly Version](#)[Interactive Discussion](#)

Benefit of Ceilometers

M. Wiegner et al.

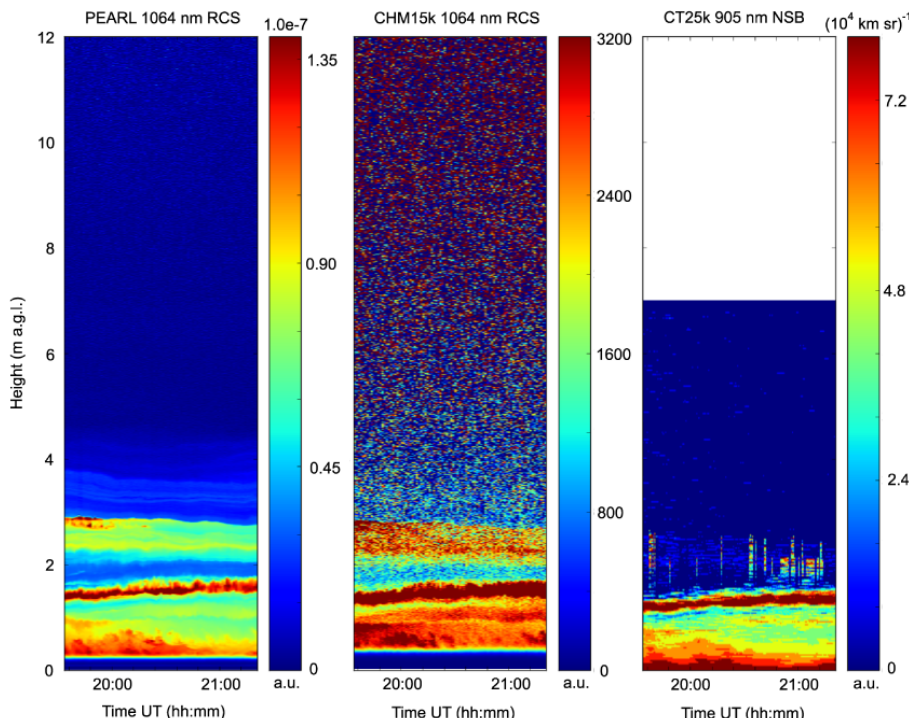


Fig. 10. Same as Fig. 10, but 25 April 2010 from 19:36 to 21:15 UTC.

Title Page	Abstract	Introduction
Conclusions	References	
Tables	Figures	
◀	▶	
◀	▶	
Back	Close	
Full Screen / Esc		

[Printer-friendly Version](#)[Interactive Discussion](#)

Benefit of Ceilometers

M. Wiegner et al.

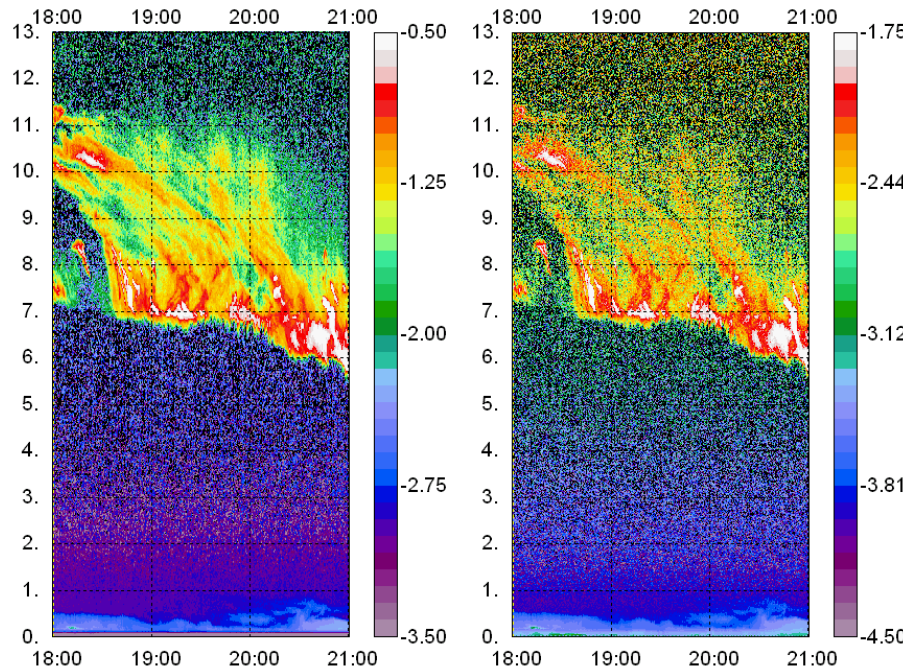


Fig. 11. Range corrected signal from 18 January 2012, 18:00 to 21:00 UTC of Jenoptik CHM15kx (left) and Vaisala CL51 (right) at Munich; logarithmic color scale in arbitrary units.

Title Page	Abstract	Introduction
Conclusions	References	
Tables	Figures	
◀	▶	
◀	▶	
Back	Close	
Full Screen / Esc		

[Printer-friendly Version](#)[Interactive Discussion](#)

Benefit of Ceilometers

M. Wiegner et al.

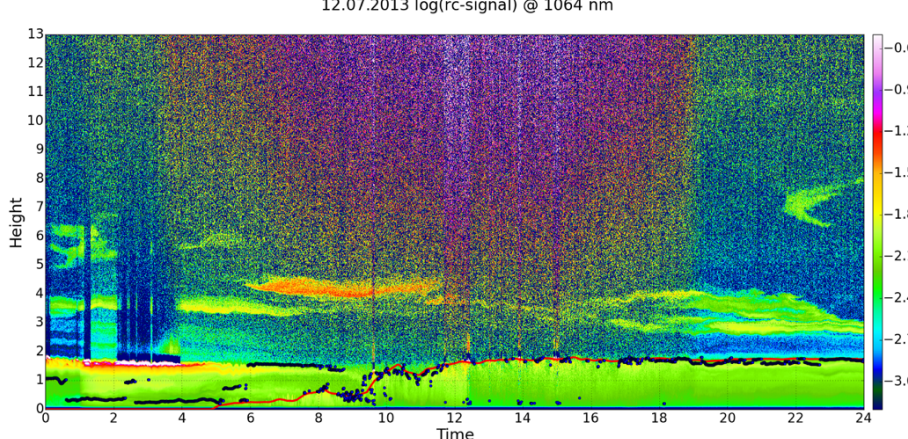


Fig. 12. Time height cross section of the range corrected signal (logarithmic color scale in arbitrary units) of a CHM15kx ceilometer (12 July 2013, Munich, $\lambda = 1064$ nm). The height of the mixing layer z_{ml} as derived from STRAT (blue) and the hybrid algorithm (red) is indicated. Time is given in UTC, height in km.

Title Page	Abstract	Introduction
Conclusions	References	
Tables	Figures	
◀	▶	
◀	▶	
Back	Close	
Full Screen / Esc		

[Printer-friendly Version](#)[Interactive Discussion](#)

Benefit of Ceilometers

M. Wiegner et al.

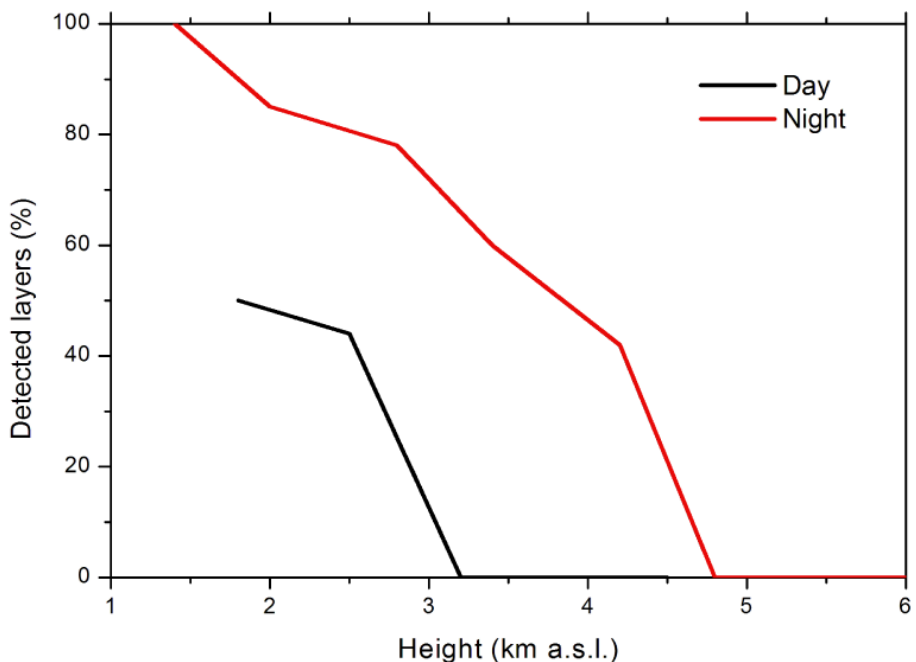


Fig. 13. Percentage of elevated layers observed by MUSA (EARLINET-lidar) in 2010 at CIAO Observatory (Potenza, Italy) that are also detected by the CHM15k ceilometer.

- [Title Page](#)
- [Abstract](#) [Introduction](#)
- [Conclusions](#) [References](#)
- [Tables](#) [Figures](#)
- [◀](#) [▶](#)
- [◀](#) [▶](#)
- [Back](#) [Close](#)
- [Full Screen / Esc](#)
- [Printer-friendly Version](#)
- [Interactive Discussion](#)



Benefit of Ceilometers

M. Wiegner et al.

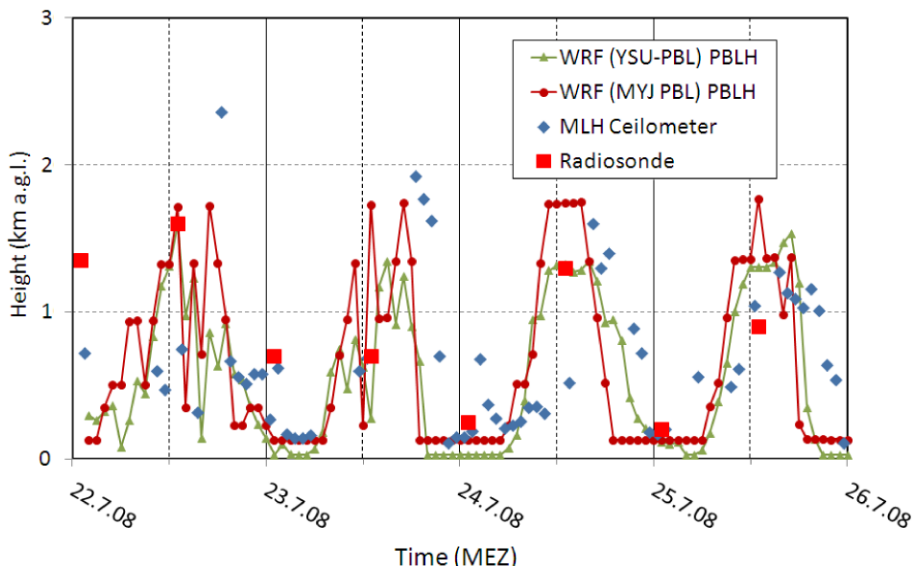


Fig. 14. Comparison of PBL heights derived from WRF/Chem simulations applying PBL-schemes as indicated and from ceilometer data in Augsburg for the time period from 22 July to 25 July 2008. The red squares indicate the mixing layer heights derived from radiosonde ascents at Oberschleißheim, Germany.

- [Title Page](#)
- [Abstract](#) [Introduction](#)
- [Conclusions](#) [References](#)
- [Tables](#) [Figures](#)
- [◀](#) [▶](#)
- [◀](#) [▶](#)
- [Back](#) [Close](#)
- [Full Screen / Esc](#)
- [Printer-friendly Version](#)
- [Interactive Discussion](#)